



This discussion paper is/has been under review for the journal Geoscientific Model Development (GMD). Please refer to the corresponding final paper in GMD if available.

Model–data fusion across ecosystems: from multi-site optimizations to global simulations

S. Kuppel^{1,2}, P. Peylin¹, F. Maignan¹, F. Chevallier¹, G. Kiely³, L. Montagnani⁴,
and A. Cescatti⁵

¹Laboratoire des Sciences du Climat et de l'Environnement, UMR8212 CEA-CNRS-UVSQ,
91191 Gif-sur-Yvette cedex, France

²Grupo de Estudios Ambientales, IMASL – CONICET/Universidad Nacional de San Luis,
Ejército de los Andes 950, D5700HHW San Luis, Argentina

³Civil and Environmental Engineering Department, and Environmental Research Institute,
University College Cork, Cork, Ireland

⁴Forest Services, Autonomous Province of Bolzano, 39100 Bolzano, Italy

⁵European Commission, Joint Research Center, Institute for Environment and Sustainability,
Ispra, Italy

Received: 17 March 2014 – Accepted: 20 April 2014 – Published: 6 May 2014

Correspondence to: S. Kuppel (skuppel@unsl.edu.ar)

Published by Copernicus Publications on behalf of the European Geosciences Union.

Title Page

Abstract

Introduction

Conclusions

References

Tables

Figures

◀

▶

◀

▶

Back

Close

Full Screen / Esc

Printer-friendly Version

Interactive Discussion



Abstract

This study uses a variational data assimilation framework to simultaneously constrain a global ecosystem model with eddy covariance measurements of daily net carbon (NEE) and latent heat (LE) fluxes from a large number of sites grouped in seven plant functional types (PFTs). It is an attempt to bridge the gap between the numerous site-specific parameter optimization works found in the literature and the generic parameterization used by most land surface models within each PFT. The present multi-site approach allows deriving PFT-generic sets of optimized parameters enhancing the agreement between measured and simulated fluxes at most of the sites considered, with performances often comparable to those of the corresponding site-specific optimizations. Besides reducing the PFT-averaged model–data root-mean-square difference (RMSD) and the associated daily output uncertainty, the optimization improves the simulated CO₂ balance at tropical and temperate forests sites. The major site-level NEE adjustments at the seasonal scale are: reduced amplitude in C₃ grasslands and boreal forests, increased seasonality in temperate evergreen forests, and better model–data phasing in temperate deciduous broadleaf forests. Conversely, the poorer performances in tropical evergreen broadleaf forests points to deficiencies regarding the modeling of phenology and soil water stress for this PFT. An evaluation with data-oriented estimates of photosynthesis (GPP) and ecosystem respiration (R_{eco}) rates indicates distinctively improved simulations of both gross fluxes. The multi-site parameter sets are then tested against CO₂ concentrations measured at 53 locations around the globe, showing significant adjustments of the modeled seasonality of atmospheric CO₂ concentration, whose relevance seems PFT-dependent, along with an improved interannual variability. Lastly, a global scale evaluation with remote sensing NDVI measurements indicates an improvement of the simulated seasonal variations of the foliar cover for all considered PFTs.

Generic model optimization across ecosystems

S. Kuppel et al.

[Title Page](#)

[Abstract](#)

[Introduction](#)

[Conclusions](#)

[References](#)

[Tables](#)

[Figures](#)

◀

▶

[Back](#)

[Close](#)

[Full Screen / Esc](#)

[Printer-friendly Version](#)

[Interactive Discussion](#)



1 Introduction

Land surface models (LSMs) have been tools of growing importance in the continuous effort to develop comprehensive Earth system models which help to understand the effects of changes in land surface processes and land-use practices upon biogeochemical (carbon, water, nutrients) and energy cycles, and more generally upon the Earth's climate (Cramer et al., 2001; Friedlingstein et al., 2006; Sitch et al., 2008). With the goal of improving accuracy and realism, the increasing number and range of scale of the processes included in mechanistic LSMs result in a growing number of parameters associated with the corresponding model equations (Pitman, 2003). Some parameters are easily identified with a given physical process (and can sometimes be measured); others are purely empirical and account for a variety of processes embodied in a few equations, yet to be refined. In both cases, obvious computational and complexity limits have traditionally led model developers to use broad classes of soil and vegetation types, for which typical, generic parameter values are assigned (e.g., Sellers et al., 1996).

One difficulty is in scaling up the leaf- and plant-level measurements of physical parameters for ecosystem-scale simulations (Bonan et al., 2012; Jarvis, 1995). Besides, the variety of species within each of the 10 to 20 plant functional types (PFTs) typically used by most models makes the choice of a representative parameter value critical, thus adding significant uncertainty to the model outputs. In this context, parameter optimization methods have been increasingly used to calibrate model parameters and reduce the associated uncertainty. The criterion is to minimize the misfit between simulation outputs and observed data (Raupach et al., 2005). As for ecosystem models, eddy covariance measurements provide direct, near-continuous, in situ observations of carbon dioxide, water and energy exchanges between the canopy and the atmosphere (Balocchi, 2008; Balocchi et al., 2001). This measurement method has been applied across an extensive global network (560 sites as of October 2013), spanning a wide range of ecosystems and climates (<http://fluxnet.ornl.gov/>).

Generic model optimization across ecosystems

S. Kuppel et al.

[Title Page](#)

[Abstract](#)

[Introduction](#)

[Conclusions](#)

[References](#)

[Tables](#)

[Figures](#)

◀

▶

[Back](#)

[Close](#)

[Full Screen / Esc](#)

[Printer-friendly Version](#)

[Interactive Discussion](#)



Over the last decade, numerous studies with various LSMs have used this available information to derive sets of parameters that significantly improve the model–data fit, with optimization approaches ranging from simple parameter adjustments to rigorous data assimilation frameworks (e.g., Braswell et al., 2005; Carvalhais et al., 2010;

5 Keenan et al., 2012; Knorr and Kattge, 2005; Reichstein et al., 2003; Santaren et al., 2007; Thum et al., 2008; Wang et al., 2007, 2001; Williams et al., 2009). However, most of these efforts have focused on model calibration at individual sites. It often results in model parameters overly tuned to the specifics of a particular site given the small spatial footprint of each flux tower (typically a few hectares). Only recently, some
10 15 studies started to assess through optimization the generic nature of model parameters within PFTs. The benefit of a set of parameters derived at one site was evaluated for simulations at a similar site (Medvighy et al., 2009; Verbeeck et al., 2011) and over the surrounding region (Medvighy and Moorcroft, 2011), with encouraging results. In parallel, two independent efforts simultaneously used data constraints from several sites to assess the degree of improvement of the simulated fluxes depending on the “generic criterion” used for the optimized parameters (Groenendijk et al., 2011; Kuppel et al., 2012). The study of Groenendijk et al. (2011), conducted at over a hundred locations across several PFTs, found that the cross-site parameter variability after optimization explained the poorer performances of grouping sites by PFT, while no such
20 discrepancy appeared in Kuppel et al. (2012), a study limited to temperate deciduous broadleaf forests.

Building on the optimization procedure developed by Kuppel et al. (2012), the present work assesses the potential of the multi-site assimilation of carbon net ecosystem exchange (NEE) and latent heat (LE) flux measurements in a process-based terrestrial ecosystem model (ORCHIDEE). The objective is to improve site-scale simulations of carbon and water fluxes at a large number of flux towers sites, as well as global scale simulations of vegetation phenology and terrestrial carbon balance. Specifically, we address the following questions: (1) for each of the 7 PFTs considered (out of 12 in ORCHIDEE, 5 being not covered by the measurements used here), can we find
25

Generic model optimization across ecosystems

S. Kuppel et al.

[Title Page](#)

[Abstract](#)

[Introduction](#)

[Conclusions](#)

[References](#)

[Tables](#)

[Figures](#)

◀

▶

◀

▶

[Back](#)

[Close](#)

[Full Screen / Esc](#)

[Printer-friendly Version](#)

[Interactive Discussion](#)



a generic set of optimized parameters that enhance the model–data fit at all sites? (2) How well does the multi-site approach compare to site-specific optimizations? (3) What are the main improvements introduced by the optimization procedure from seasonal to annual time scales: daily error, model–data bias, seasonal cycle amplitude and/or phase? (4) Which processes remain poorly captured by the model after optimization? (5) Have the eddy-covariance-constrained sets of multi-site parameters a notable impact on global scale simulations?

Section 2 presents the ecosystem model, the data assimilation system, and the eddy covariance measurements used in this study, as well the supplementary datasets and models. The results are presented and discussed in Sect. 3, successively dealing with the model–data fit at the site level (Sect. 3.1), the comparison between multi- and single-site results (Sect. 3.2), the uncertainties of modeled NEE and LE (Sect. 3.3). Then are evaluated the impact of the derived multi-site parameterization upon the site-scale simulation of photosynthesis and ecosystem respiration rates (Sect. 3.4), and at the global scale upon the simulated seasonality and interannual variability of atmospheric CO₂ concentration (Sect. 3.5.1) and finally upon the seasonality of vegetation activity (Sect. 3.5.2).

2 Materials and methods

2.1 Vegetation model and optimized parameters

The biogeochemical vegetation model used in this study is ORCHIDEE (Organizing Carbon and Hydrology in Dynamic Ecosystems, Krinner et al., 2005). It calculates the water, energy and carbon fluxes between the land surface and the atmosphere at a half-hourly time step. The exchange of carbon and water during photosynthesis and the energy balance are treated every 30 min, while carbon allocation, autotrophic respiration, foliar onset and senescence, mortality and soil organic matter decomposition are computed on a daily time step. The soil hydrology follows a double-bucket

Generic model optimization across ecosystems

S. Kuppel et al.

[Title Page](#)[Abstract](#)[Introduction](#)[Conclusions](#)[References](#)[Tables](#)[Figures](#)[◀](#)[▶](#)[◀](#)[▶](#)[Back](#)[Close](#)[Full Screen / Esc](#)[Printer-friendly Version](#)[Interactive Discussion](#)

scheme (Ducoudré et al., 1993) and its impact on stomatal conductance is described in Krinner et al. (2005). The reader is referred to previous publications for the standard equations of ORCHIDEE (e.g., Kuppel et al., 2012). As in most biogeochemical models, the vegetation is grouped into several PFTs, 12 in the case of ORCHIDEE, excluding bare soil. Except for the modeled phenology (Botta et al., 2000), the equations governing the different processes are generic across PFTs, but with specific parameter values for each vegetation class. When used in “grid-point mode” at a given site, we force the model with the corresponding half-hourly gap-filled meteorological data measured at the flux towers. At the global scale, the global ERA-Interim meteorology (Dee et al., 2011) is used as forcing and the model outputs are calculated at a $0.72^\circ \times 0.72^\circ$ resolution. In this case the global PFT map is computed at the spatial resolution of the forcing fields, from an original vegetation map available at 5 km, which is derived from a high-resolution IGBP AVHRR global land dataset (Eidenshink and Faundeen, 1994) and uses 94 ecosystem classes (Olson, 1994). Importantly, the modeled carbon pools are initially brought to equilibrium by cycling the available meteorological forcing over several centuries (spin up procedure), with the prior parameterization of the model. This procedure ensures a net carbon flux close to zero over annual-to-decadal timescales.

Table 1 presents the PFT-generic parameters used in this study, which have been chosen based on the optimized parameters set used in Kuppel et al. (2012) and additional sensitivity analyses. As our emphasis is on adjusting the carbon cycle, there are significantly more optimized parameters leveraging on photosynthesis and respiration processes than, for instance, on the energy balance. We also included two additional parameters to optimize the initial state of the model provided by the spin up procedure, which are (1) a common multiplier of the initial carbon pool content, by default equal to one, and (2) the initial leaf area index (LAI) of non-deciduous PFTs, by default taken from the spin up outputs. Both parameters are considered as site-specific, since the soil organic carbon content is closely related to the local land-use history, while the foliar cover of evergreen and herbaceous species directly relates to vegetation history

at the site level. One consequence is that they cannot be spatially extrapolated, thus the global simulations performed for evaluation (see Sect. 2.4) use the default value of these last two parameters.

2.2 Data assimilation system

- 5 The model parameters are optimized using the variational data assimilation method described in Kuppel et al. (2012). Assuming a Gaussian distribution for errors on the parameters, the model outputs and the measured data, the optimized set of parameters corresponds to the minimization of the following Bayesian cost function $J(\mathbf{x})$ (Tarantola, 2005):

10
$$J(\mathbf{x}) = \frac{1}{2} \left[(\mathbf{y} - H(\mathbf{x}))^T \mathbf{R}^{-1} (\mathbf{y} - H(\mathbf{x})) + (\mathbf{x} - \mathbf{x}_b)^T \mathbf{P}_b^{-1} (\mathbf{x} - \mathbf{x}_b) \right], \quad (1)$$

which quantifies both the misfit between modeled and observed fluxes, and the misfit between a priori and optimized parameters. \mathbf{x} is the vector of unknown parameters, \mathbf{x}_b the vector of background (i.e., here, prior) parameter values, $H(\mathbf{x})$ the vector of modeled fluxes, \mathbf{y} the vector of observed fluxes, while \mathbf{P}_b and \mathbf{R} are the prior covariance matrices of parameter errors and observation errors, respectively.

15 The cost function is iteratively minimized with the gradient-based algorithm L-BFGS-B, which allows prescribing boundaries for each variable to optimize (Byrd et al., 1995). At each iteration, the gradient of the cost function $J(\mathbf{x})$ is computed with respect to all parameters, mostly using the Tangent Linear (TL) model of ORCHIDEE generated with the automatic differentiator tool TAF (Transformation of Algorithms in Fortran, see 20 Giering et al., 2005). Exceptions concern two phenological parameters, $K_{\text{pheno,crit}}$ and c_{Tsenes} (see Table 1), where the threshold functions prevent the use of a linear approximation. In these cases we use a finite-difference approach with prescribed perturbation steps respectively equal to 4 % and 2 % of the allowed variation range. The recent work 25 of Santaren et al. (2013) with the same ecosystem model highlighted the risk of converging towards a local minimum within a site-specific variational optimization. In our

[Title Page](#)

[Abstract](#)

[Introduction](#)

[Conclusions](#)

[References](#)

[Tables](#)

[Figures](#)

◀

▶

[Back](#)

[Close](#)

[Full Screen / Esc](#)

[Printer-friendly Version](#)

[Interactive Discussion](#)





case, preliminary tests within three PFTs (tropical and temperate evergreen broadleaf forests, and temperate deciduous broadleaf forests) allowed us to verify that the convergence of our multi-site approach barely depends on the choice of the first-guess values assigned to the optimized parameters. However, such robustness is not guaranteed with the site-specific approach, and potential convergence issues are discussed in the results section.

Once the cost function reaches the minimum, the posterior parameter error variance matrix \mathbf{P}_a is explicitly calculated from the prior error covariance matrices (\mathbf{P}_b and \mathbf{R}) and the Jacobian of the model H at the minimum of the cost function (\mathbf{H}_∞), using the linearity assumption (Tarantola, 2005):

$$\mathbf{P}_a = \left[\mathbf{H}_\infty^T \mathbf{R}^{-1} \mathbf{H}_\infty + \mathbf{P}_b^{-1} \right]^{-1} \quad (2)$$

The prior parameter error covariance matrix \mathbf{P}_b is diagonal as prior uncertainties are supposed to be uncorrelated between parameters. The prior standard deviation for each parameter is equal to 1/6 of the range between lower and higher boundaries. The latter have been carefully specified following the physical and empirical expertise of the ORCHIDEE modelers, based on literature reviews or databases (such as TRY, Kattge et al., 2011).

In the prior observation error covariance matrix \mathbf{R} , we include both the random error on the measurements and the model error, the latter stemming from missing/inadequate process representation in the structural equations of the ecosystem model. Although the measurements error is known not to be constant (e.g. Richardson et al., 2008), a previous study using the ORCHIDEE model suggested that the model component dominates the observation error budget (Kuppel et al., 2013). The variances in \mathbf{R} are chosen constant at a given site for each type of data (NEE and LE), equal to the mean square difference between the prior model and the observations. We also choose for simplicity to keep \mathbf{R} diagonal, based on the rapid decline of the model error autocorrelation beyond the first lag day (Kuppel et al., 2013).

2.3 Assimilated eddy covariance flux data

We use the eddy covariance data provided by 78 flux towers of the FLUXNET global network (Balocchi, 2008), representative of seven of the 12 vegetated PFTs defined in the ORCHIDEE model (see Table 2). All the sites of a given dominant ecosystem

- are located in the same geographical hemisphere, which makes seasonal analyses easier. These observations derive from standard flux data processing methodologies (correction, gap-filling and partitioning) of the *La Thuile* dataset (Papale, 2006). From the large amount of available site-years in this dataset, our selection was driven by several requirements, the first of these being a minimum vegetation cover of 70 % by the dominant PFT within each tower footprint, based on site-level information. Then were discarded the sites where measurements show a significant disagreement with the prior simulation outputs, as it suggests strong model structural deficiencies that make the parameter optimization pointless. Lastly, we selected at each site the longest data segment of consecutive years without gaps larger than a few weeks. Where measurements of the ground heat flux (G) were available, the monthly energy balance was closed with a correction factor then half-hourly-interpolated and applied to the latent heat (LE) and sensible heat (usually called H) fluxes, according to the Bowen ratio technique (Twine et al., 2000). The half-hourly, gap-filled measured fluxes of net ecosystem exchange (NEE) and LE are then used to compute daily means. We chose to assimilate daily-averaged observations and not half hourly measurements so as to focus the optimization on time scales ranging from seasonal to annual variations, and to take advantage of the rapidly-decreasing autocorrelation of gap-filled half-hourly fluxes (Lasslop et al., 2008). In order not to give too much weight to data estimated from gap-filling as compared to measured data, each daily observation error is inflated by a factor $1 + 0.5k$, where k is the daily fraction of half-hourly data estimated from gap-filling. We also checked that the gaps still remaining after the gap-filling were distributed evenly over the course of the day. The individual days with more than 20 % of these “ultimate” gaps were not included in the assimilation.

Generic model optimization across ecosystems

S. Kuppel et al.

Title Page

Abstract

Introduction

Conclusion:

References

Tables

Figures



Back

Close

Full Screen / Esc

[Printer-friendly Version](#)

Interactive Discussion





The eddy covariance data are compared to the simulated fluxes in terms of RMSD and bias. In addition, for the six non-tropical PFTs we use a curve fitting procedure (composed of a polynome of degree 2 and four harmonics) to decompose the fluxes into their trends and mean seasonal cycles following (Thoning et al., 1989). The de-

5 detrended smooth seasonal cycle is used to estimate the ratio between the average annual amplitude of the simulated and observed fluxes, as well as a model phase coefficient defined as

$$C_{\text{phase}} = 1 - \frac{|e_{\text{sim}} - e_{\text{obs}}| + |b_{\text{sim}} - b_{\text{obs}}|}{e_{\text{obs}} - b_{\text{obs}}} \quad (3)$$

Here, b_i and e_i are respectively defined as the first and last day of the year when the

10 detrended smooth curve crosses the zero line. In tropical evergreen broadleaf forests, the phase and amplitude diagnostics presented above are not applied, due to the lack of a marked seasonal cycle. Instead, the predictive power of the simulations is evaluated using the Nash–Sutcliffe model efficiency coefficient (Nash and Sutcliffe, 1970):

$$15 \quad NSE = 1 - \frac{\sum_{t=1}^T (F_{\text{sim}}^t - F_{\text{obs}}^t)^2}{\sum_{t=1}^T (F_{\text{obs}}^t - \bar{F}_{\text{obs}})^2} \quad (4)$$

where F_i^t is the value of the simulated or observed flux at the time step t , and \bar{F}_{obs} the mean observed flux.

2.4 Evaluation tools

20 The model is evaluated at the sites using the two components of NEE: the gross primary productivity (GPP) and the ecosystem respiration rate (R_{eco}), both estimated via the flux-partitioning method described in Reichstein et al. (2005). This method extrapolates nighttime measurement of NEE, representing nighttime R_{eco} , into daytime R_{eco}

using a short-term-calibrated temperature response function. GPP is then derived as the difference between R_{eco} and NEE. We acknowledge that GPP and R_{eco} are not fully independent data (with respect to the assimilated NEE) and are essentially model-derived estimates somewhat conditional on our underlying assumptions, and it will be kept in mind during the analysis.

Additionally, measurements of the Normalized Difference Vegetation Index (NDVI) made by the MODIS instrument are used to evaluate the simulated phenology at the global scale. From 2000 to 2010, the calculated reflectances (from measured irradiances) have been corrected for atmospheric absorption and scattering (Vermote et al., 2002) and directional effects (Vermote et al., 2009) in order to obtain a daily NDVI product with a 5 km spatial resolution. In this study, spatial averaging is used to match the ERA-Interim resolution ($0.72^\circ \times 0.72^\circ$) used for the global scale simulations. Because it is directly derived from surface reflectances, we preferred NDVI to other satellite products such as FAPAR or LAI, the latter requiring intermediate processing steps usually involving radiative transfer models, and thus possibly adding uncertainty to the retrieved data (Garrigues et al., 2008). Following Maignan et al. (2011), we then calculate the Pearson correlation factor between the times series of measured NDVI and the Fraction of Absorbed Photosynthetically Active Radiation (FAPAR) modeled by ORCHIDEE, at the weekly time scale during the period 2000–2010. FAPAR has been estimated from modeled LAI with a simple Beer’s law:

$$FAPAR = 1 - \exp(-0.5 \times LAI) \quad (5)$$

The link between simulations and measurements is made by spatially averaging the latter to reach the resolution of the vegetation model (i.e. that of the ERA-Interim forcing). For each of the seven PFTs considered, we restrict our correlation computation to the model boxes where the PFT's cover fraction exceeds 50 % and where both NDVI and FAPAR time-series exhibit a visible seasonal cycle (i.e. with a standard deviation larger than 0.04).

Generic model optimization across ecosystems

S. Kuppel et al.

Title Page

Abstract

Introduction

Conclusion:

References

Tables

Figures



Back

Close

Full Screen / Esc

[Printer-friendly Version](#)

Interactive Discussion



Generic model optimization across ecosystems

S. Kuppel et al.

[Title Page](#)

[Abstract](#)

[Introduction](#)

[Conclusions](#)

[References](#)

[Tables](#)

[Figures](#)

[◀](#)

[▶](#)

[◀](#)

[▶](#)

[Back](#)

[Close](#)

[Full Screen / Esc](#)

[Printer-friendly Version](#)

[Interactive Discussion](#)



Lastly, the simulated global NEE fluxes are output at the daily timescale and spatially averaged from the ERA-Interim grid ($0.72^\circ \times 0.72^\circ$) to a $2.5^\circ \times 3.75^\circ$ resolution (latitude, longitude). The LMDz atmospheric transport model (Hourdin et al., 2006) was used at this resolution to convert these terrestrial fluxes into monthly atmospheric CO₂ concentrations, during the period 1989 to 2009. In order to complete the carbon balance at the planetary scale, we also transport the global oceanic and fossil net carbon fluxes respectively taken from a climatology (Takahashi et al., 2009) and from the EDGAR database (<http://edgar.jrc.ec.europa.eu>). The contribution of biomass burning is neglected, because re-growth of burnt vegetation is not accounted for in this version of ORCHIDEE, and so are the evasion of CO₂ from aquatic bodies and emissions from harvested wood and agricultural products. The transported fluxes are evaluated using 53 smoothed record of atmospheric CO₂ concentrations (C_{CO_2}) over the globe (Supplement Table S1) (GLOBALVIEW-CO₂, 2013). As the optimization of the initial soil carbon content cannot be spatially extrapolated for global simulations (see Sect. 2.1), the modeled trend of C_{CO_2} is not evaluated. Rather, we focus on the seasonal analysis and use the curve-fitting procedures of (Thoning et al., 1989) to extract the detrended seasonal signal of C_{CO_2} . In addition, we identify the contributions of 11 sub-continental regions to the simulated atmospheric CO₂ concentration at each station by independently transporting the fluxes from each following area: boreal North America, temperate North America, tropical America, South America, Europe, northern Africa, southern Africa, boreal Asia, temperate Asia, tropical Asia, and Australia (e.g., Fig. 1 in Gurney et al., 2003). The simulated interannual variability of the C_{CO_2} is evaluated using the model–data RMSD of monthly anomaly, from the detrended smooth seasonal signal calculated above:

$$C_{CO_2, \text{anom}} = C_{CO_2, \text{month}} - \langle C_{CO_2, \text{month}} \rangle_{\text{all years}} \quad (6)$$

where $\langle C_{CO_2, \text{month}} \rangle_{\text{all years}}$ is the all-time average, for each month of the year.

3 Results and discussion

3.1 Site-level simulation of carbon and water fluxes

Figure 1 shows the average corrections brought by the optimization to the modeled NEE fluxes (with negative values meaning carbon uptake), grouped by dominant PFT, in terms of RMSD and bias between simulations and measured data, also showing the PFT-averaged mean seasonal cycles. The largest reductions of model–data RMSD are found in temperate and boreal broadleaf forests (TempEBF, TempDBF and BorDBF), where the two optimization scenarios (single- and multi-site) decrease the misfit by more than 25 % compared with the prior (unoptimized) model. In temperate needleleaf forests (TempENF) and C₃ grasslands (C3grass), the RMSD reduction exceeds 30 % for single-site optimizations, but the corresponding multi-site sets of parameters reduce this value to less than 20 %. The improvements are less significant in tropical evergreen broadleaf forests (TropEBF) and boreal evergreen needleleaf forests (BorENF), where the reductions of misfit remain between 9 and 15 %. Figure 1b shows that the NEE is on average overestimated by the prior model for all PFTs. This feature is even more striking in ecosystems which are marked sinks of carbon (according to the average measured carbon balance, not shown), here tropical and temperate forests. This positive bias is an artifact from the model initialization procedure, which brings each simulated site to a near equilibrium (see Sect. 2.1). It is significantly corrected by the optimization, notably via the scaling of the initial carbon pool content at each site (parameter K_{soilC} in Table 1), one consequence being a clear reduction of the respiration during the winter of temperate and boreal ecosystems and grasslands sites in agreement with the measured data (Fig. 1c).

Figure 2 shows that the simulation of the latent heat flux (LE) is overall less improved by the optimizations than that of the net carbon flux, keeping however in mind the problem of energy balance closure discussed in Sect. 2.3. The reduction of RMSD is the highest on average at TempDBF sites with values 24 % below the prior value, while decreases of 15 to 19 % are found at TempEBF and BorENF sites. The effect of

[Title Page](#)[Abstract](#)[Introduction](#)[Conclusions](#)[References](#)[Tables](#)[Figures](#)[◀](#)[▶](#)[Back](#)[Close](#)[Full Screen / Esc](#)[Printer-friendly Version](#)[Interactive Discussion](#)

Title Page	
Abstract	Introduction
Conclusions	References
Tables	Figures
	
	
Back	Close
Full Screen / Esc	
Printer-friendly Version	
Interactive Discussion	

the optimization is the weakest on average at sites located in TempENF and C3grass ecosystems. These weaker performances regarding LE flux indicate that the energy and water cycles in the ORCHIDEE model involve other relevant parameters not optimized here, and possibly that the structural equations bear a significant error. Notably, we include in the optimization only one parameter that directly controls the soil evaporation ($Z_0_{\text{overheight}}$, see Table 1), and there is for example no constraint on the calculation of the surface temperature, a key component of the energy balance.

At the seasonal scale, Fig. 3a shows that large reductions (in relative value) of the simulated mean seasonal NEE amplitude are found in boreal evergreen needleleaf and deciduous broadleaf forests and C₃ grasslands. The average correction is somewhat exaggerated in the two former cases and relatively accurate in the latter case. Conversely, the seasonal NEE variations are consistently amplified by the optimization in temperate evergreen needleleaf and broadleaf forests. However, the averaged model–data phasing is only weakly modified for the five aforementioned PFTs, with the exception of the site-specific improvements at TempENF and C3grass sites. Besides, considering the mild correction of the model–data biases in BorENF, BorDBF and C3grass (Fig. 1b), one can deduce that most of the reduction of RMSD discussed earlier is for these three PFTs due to an improvement of the simulated NEE amplitude after the optimization.

In temperate deciduous broadleaf forests, the simulated pattern of NEE is chiefly improved via a better phased seasonal cycle, as shown by the increased phase score, which was already close to one before optimization. An earlier study at a similar set of sites of the same PFT showed that the optimization scheme tends to correct the overall prior model overestimation of the growing season length (Kuppel et al., 2012). On the other hand, the simulated seasonal amplitude of NEE is barely changed after optimization, as the corrected flux overestimations in winter and summer tend to cancel out, with a PFT-averaged seasonal amplitude remaining smaller than that of the observed data (Figs. 1c and 3).

Regarding the latent heat flux, Fig. 3b shows that the optimization has generally a weaker effect on the simulated LE average phase and amplitude than in the case of NEE. In most cases the correction brought by the optimization barely affects the modeled phase, but improves the seasonal amplitude. We notice that the LE seasonal cycle 5 is most often flattened as compared to the prior model in agreement with the observations, except for the inconsistent amplification at TempEBF sites and the over-reduction after the site-specific optimization in C₃ grasslands. The weak phase correction might be related to the soil evaporation component of the latent heat flux, on which the optimization has a limited leverage as mentioned earlier in this section, while the transpiration rate is tightly linked to GPP. It would also explain the generally lower phase 10 coefficient in deciduous ecosystems (Fig. 3), where soil evaporation is a potentially significant component of LE during leaf onset and senescence.

Besides, applying the Nash–Sutcliffe model efficiency coefficient (NSE, see Eq. 4) to all sites shows that TropEBF is the only PFT studied here where the PFT-averaged 15 value of this metric remains below zero after optimization for both fluxes, with $NSE_{NEE} = [-2.77, -1.99, -1.83]$ and $NSE_{LE} = [-0.64, -0.35, -0.52]$ in prior, multi-site and site-specific cases, respectively (other PFT values not shown). It means that after optimization the model–data mean square error is still larger than the variance of the observations, or, in other words, that the observed mean is on average a better predictor 20 than the model outputs. Figure 1 shows that for TropEBF the prior model simulates an unobserved increase of NEE from sink to source around July, and the simultaneous decrease of LE (Fig. 2) points towards an unrealistic simulated drought stress during this period of the year, the driest at most sites of this PFT. The optimization barely corrects the NEE variations during the dry season, although a more realistic LE flux 25 is simulated after the multi-site optimization. An earlier optimization study at a site of the same PFT highlighted the need for a much deeper soil water reservoir along with a more linear root profile than that parameterized in the prior model, in order to account for the ability of tropical evergreen forests to maintain high photosynthesis and transpiration during the dry season (Verbeeck et al., 2011). Our multi-site parameterization

[Title Page](#)[Abstract](#)[Introduction](#)[Conclusions](#)[References](#)[Tables](#)[Figures](#)[◀](#)[▶](#)[◀](#)[▶](#)[Back](#)[Close](#)[Full Screen / Esc](#)[Printer-friendly Version](#)[Interactive Discussion](#)

of the processes dealing with soil water availability goes in that direction, with values of soil water depth, root profile and water stress coefficient respectively adjusted from 2 to 2.38 ± 0.065 m, from 0.8 to 0.72 ± 0.095 m⁻¹ and from 6 to 6.5 ± 1.06 (Table 1). These corrections from the prior parameterization remain however insufficient, as shown by the poorly realistic optimized seasonal cycle of NEE in Fig. 1. On the other hand, Verbeeck et al. (2011) also pointed at the structural inconsistency in the standard ORCHIDEE model for tropical evergreen forests: the phenological scheme notably neglects the leaf renewal at the transition between wet and dry season (Chave et al., 2010) and the hydric stress calculation ignores the role of groundwater (Miguez- Macho and Fan, 2012), while these mechanisms possibly explain the high subsequent photosynthesis and transpiration rates often observed (De Weirdt et al., 2012). Concerning the LE flux, the optimization brings somewhat limited, yet consistent changes, while the reduction of daily uncertainty is modest, indicating a poor level of constraint by the observations used. It suggests either significant errors in the model equations, or that relevant, poorly known parameters, have not been considered.

3.2 Single-site vs. multi-site

It can be noticed in Figs. 1–3 that there is a general consistency across PFTs between RMSD reductions introduced by multi-site and site-specific optimizations, with some exceptions in TempENF and most notably C3grass where the average site-specific RMSD reduction is twice as large for NEE, while there is almost no average multi-site RMSD decrease for LE. Although the large number of sites selected for this last PFT and the associated inter-site variability calls for prudence when considering average seasonal flux variations, it is worth noting that C₃ grasslands are here the only PFT generically spanning such a diversity of climates. The reported discrepancy might thus indicate a need for additional classes of C₃ grasslands in the model, at least with a climatic regionalization and ideally taking also into account pedologic conditions and management practices.

[Title Page](#)[Abstract](#)[Introduction](#)[Conclusions](#)[References](#)[Tables](#)[Figures](#)[◀](#)[▶](#)[◀](#)[▶](#)[Back](#)[Close](#)[Full Screen / Esc](#)[Printer-friendly Version](#)[Interactive Discussion](#)

More generally, one would expect better efficiency from a site-specific scheme than with a multi-site approach, given that grouping sites with different characteristics introduces conflicting constraints on the model equations, along with the fact that the RMSD is the criterion used in the optimization procedure (as the prior covariance matrix in the

5 cost function of Eq. (1) is chosen diagonal, see Sect. 2.2). It is true most of the time, except notably for NEE in boreal deciduous broadleaf forests and LE at TropEBF, TempEBF and BorENF sites where the multi-site optimization results on average in larger RMSD decreases than the site-specific approach. In these cases, Figs. 1 and 2 show that it stems from unchanged local RMSD after the site-specific optimization at a few
10 sites of these particular PFTs. As found by (Santaren et al., 2013), it may point to a failure of the single-site inversion algorithm to converge towards the global minimum of the cost function, possibly due to the presence of local minima. Our hypothesis is that the corresponding multi-site cost functions avoid this pitfall because they are made more regular by the larger amount of simultaneous constraints on the parameters, “smoothing out” some of the problematic local minima. Preliminary multi-site optimization
15 tests, using a few tens of random starting points, support this hypothesis, and further investigations will be needed to evaluate if this behavior is valid for all PFTs. Indeed, we acknowledge some uncertainty regarding whether or not the optimized sets of parameters correspond to the very minimum of the cost function, as the efficiency of the
20 variational optimization approach employed is conditional on a reasonable compliance with the linearity hypothesis. Stochastic methods could comparatively provide larger reductions of the cost function and a site-specific application with the same LSM showed promising results (Santaren et al., 2013), but the computational time required for an efficient convergence with more than 20 parameters and a complex model such as
25 ORCHIDEE currently makes these techniques ill-suited for a multi-site approach.

3.3 Site-scale uncertainty

In addition to improving the agreement between modeled and measured fluxes, the optimization procedure is also useful to reduce the total uncertainty associated with

Generic model optimization across ecosystems

S. Kuppel et al.

[Title Page](#)

[Abstract](#)

[Introduction](#)

[Conclusions](#)

[References](#)

[Tables](#)

[Figures](#)

◀

▶

◀

▶

[Back](#)

[Close](#)

[Full Screen / Esc](#)

[Printer-friendly Version](#)

[Interactive Discussion](#)



the modeled output variables at each site, defined as:

$$\sigma_{\text{total}} = \sqrt{\sigma_{\text{observations}}^2 + \sigma_{\text{parameters}}^2} \quad (7)$$

$\sigma_{\text{observations}}$ represents the summed contribution of two errors arising in the observation space: the measurements error and the error of the equations of the model

- 5 (see Sect. 2.2). It is not directly altered through parameter optimization, although the model component may in principle vary with the parameter values. Following Kuppel et al. (2013), $\sigma_{\text{observations}}$ is diagnosed at each site as the square root of the covariance between the time series of prior and posterior flux residuals (model minus observations). $\sigma_{\text{parameters}}$ is the parameter error contribution to the simulated fluxes, calculated
- 10 at each site, before optimization, as the average daily standard deviation of the projection in observation space of the prior error covariance matrix \mathbf{P}_b , using the model's Jacobian matrix \mathbf{H} , based on the definitions of Sect 2.2. The same is done after optimization, respectively using \mathbf{P}_a and \mathbf{H}_∞ .

Figure 4 reports the average value of σ_{total} for simulated daily NEE and LE, showing individual sites values and the corresponding PFT means as in Figs. 1 and 2. The reduction of the total NEE uncertainty varies from one PFT to another, ranging from 6 % in tropical evergreen broadleaf forests to 33 % in boreal evergreen needleleaf forests. As $\sigma_{\text{parameters}}$ is reduced by 65 to 95 % (not shown), we deduce from Eq. (7) that the weak relative decrease of σ_{total} indicates a dominance of the observation error in the

- 20 total uncertainty budget. This is for example consistent with the reported inaccuracies in the model structure for TropEBF ecosystems discussed in the previous section.

Regarding the LE flux, the mild changes from prior to posterior uncertainty means that we might face a potentially large observation error component (model + measurements) – the latter being insensitive to parameter optimization, see Sect. 2.3 – and overall that little statistical information has been gained from the optimization of the selected water cycle parameters. Indeed, our choice of parameters has been mostly driven by a model sensitivity criterion, while the actual leverage of an

Generic model optimization across ecosystems

S. Kuppel et al.

[Title Page](#)[Abstract](#)[Introduction](#)[Conclusions](#)[References](#)[Tables](#)[Figures](#)[◀](#)[▶](#)[◀](#)[▶](#)[Back](#)[Close](#)[Full Screen / Esc](#)[Printer-friendly Version](#)[Interactive Discussion](#)

optimized parameter on model outputs also depends on the uncertainty associated to this very parameter (Keenan et al., 2012; Xu et al., 2006).

Besides, one can notice that the posterior uncertainties are always slightly lower for multi-site optimization than with the site-specific approach, which is consistent with the fact that the number of assimilated data is larger in the former case than in the latter. Finally, we also found that the optimization suppresses at each site much of the temporal correlation of the flux error, which are large in the prior ORCHIDEE model (see for instance the time correlogram in the Fig. 1 of Kuppel et al., 2013). It results in a large decrease of the total yearly uncertainty from the prior model for all PFTs, by 77 to 86 % and 43 to 80 % for simulated NEE and LE flux, respectively (not shown).

3.4 Simulated GPP and respiration

Figure 5 shows the mean seasonal cycle, averaged over each PFT, for the gross carbon fluxes: photosynthesis (GPP, Fig. 5a) and ecosystem respiration (R_{eco} , Fig. 5b). The “observed” values are estimates based on a partition of the measured NEE (see Sect. 2.4). These gross carbon fluxes have not been used as constraints in the optimization procedure, but are useful as indicators of the model performance. One can first notice that the average increases of GPP at TropEBF and TempEBF sites are responsible for the NEE decrease observed in Fig. 1. It is worth noting that the results reported in Fig. 5 also confirm the inability of the model to simulate a sustained high photosynthesis rate during the dry season at TropEBF sites (see Sect. 3.1), while this feature appears in the observations estimates. At TempENF sites, the remarkable adjustment of the NEE cycle primarily derives from a reduced R_{eco} at the peak of the growing season. Both GPP and R_{eco} are consistently decreased at boreal forests and C₃ grasslands sites, although the reduction is still lower than what would be needed to match the estimates. In addition, because the respiration rate is the sole reducing component in winter and because the photosynthesis rate is more largely decreased than R_{eco} during the growing season, the net result is the reduction of the seasonal amplitude of NEE for these three PFTs. Finally there is a large, yet insufficient, decrease

of R_{eco} after the optimization in temperate deciduous broadleaf forests, notably related to the scaling of the initial carbon pool content (Sect. 3.1 and Kuppel et al., 2012), while GPP is less drastically reduced, in close agreement with the observations.

With the exception of tropical sites, this evaluation at each site with gross carbon fluxes shows that the optimization procedure is able to provide a set of parameters which improves the simulation of both assimilation and respiration processes in the ORCHIDEE model for the 7 PFTs, suggesting a partial distinction of both gross contributions from the constraint provided by the net carbon flux.

3.5 Global-scale evaluation

- One of the objectives of assimilating flux data from a large number of sites, spanning a wide range of ecosystems, is to identify generic sets of parameters that improve the simulation of carbon and water balance at the regional-to-global scale. Indeed, there is no guarantee that a set of parameters improving the simulations at an ensemble of individual sites sharing broadly common biogeochemical and biophysical characteristics, but with a limited spatial footprint, will also be beneficial for simulations at much larger scales. In this context, global simulations allow evaluation of how the constraint of eddy covariance data is propagated from one spatial scale to another, and how transferable the optimized parameterization is from grouped in situ optimizations to gridded simulations.

3.5.1 Seasonality of atmospheric CO₂ concentrations

Regarding the simulated mean seasonal cycle of atmospheric C_{CO_2} , the optimized set of parameters yields a median reduction of the model–data RMSD of 5.2 %. Among the 53 samples locations used in this study, there is a significant improvement at 27 of them with a RMSD decrease larger than 5 %, a notable degradation at 20 sites with a RMSD increase larger than 5 %, and less than a 5 % shift at the remaining 6 locations. In addition, a latitudinal clustering can be identified, as a large median improvement

[Title Page](#)[Abstract](#)[Introduction](#)[Conclusions](#)[References](#)[Tables](#)[Figures](#)[◀](#)[▶](#)[◀](#)[▶](#)[Back](#)[Close](#)[Full Screen / Esc](#)[Printer-friendly Version](#)[Interactive Discussion](#)

Generic model optimization across ecosystems

S. Kuppel et al.

[Title Page](#)[Abstract](#)[Introduction](#)[Conclusions](#)[References](#)[Tables](#)[Figures](#)[◀](#)[▶](#)[◀](#)[▶](#)[Back](#)[Close](#)[Full Screen / Esc](#)[Printer-friendly Version](#)[Interactive Discussion](#)

by 42.2 % (RMSD-wise) is found at the 3 northernmost sites (Alert, Ny-Alesund, and Barrow) and by 33.5 % at the 18 locations of the Southern Hemisphere, while there is a median degradation by 5.6 % in the rest of the Northern Hemisphere.

Figure 6 shows the mean seasonal cycle of the simulated C_{CO_2} , compared to the extended record at three locations, one in each of the latitudinal areas defined above: Alert, South Pole, and Mauna Loa, respectively. We note that the optimization tends to reduce the seasonal amplitude of C_{CO_2} , with in the Northern Hemisphere an earlier phasing for the “breathing of the biosphere”. At station Alert, there is a significant adjustment of the simulated seasonal cycle, when changing from the default to the multi-site parameterization of the ORCHIDEE model. This correction chiefly benefits the seasonal amplitude, which is decreased and becomes remarkably close to that observed. The analysis of the contribution of the 11 sub-continental regions in the simulated atmospheric signal (see Sect. 2.4), grouped in Fig. 6d in larger regions, indicates that the major terrestrial contribution to this result are changes in C_{CO_2} due to the boreal Northern Hemisphere fluxes. It is consistent with the decrease of the NEE seasonal amplitude produced by the multi-site optimization at sites in boreal evergreen needleleaf forests, boreal deciduous broadleaf forests and C₃ grasslands (see Sect. 3.1), dominant in this region. Separate global simulations using optimized parameterization for one PFT at a time show that the degraded phasing at Alert produced by the multi-site approach in Fig. 6a mainly stems from the contributions of BorENF and C₃ grasslands ecosystems (not shown). As no such average deterioration from the prior parameterization is visible for these PFTs at the site level (see Figs. 1 and 3), these results may question the representativeness of the flux measurements sites used, with respect to high-latitudes ecosystems in general.

At station South Pole, the model–data fit is also mostly enhanced after the optimization by a significant decrease of the seasonal amplitude of C_{CO_2} , which is more than twice as large in the prior simulation as in the measured data. Besides, the “regionalized” analysis indicates that the corrections are primarily due to the reduced seasonal amplitude of C_{CO_2} components from temperate South America and southern

Generic model optimization across ecosystems

S. Kuppel et al.

Title Page	
Abstract	Introduction
Conclusions	References
Tables	Figures
◀	▶
◀	▶
Back	Close
Full Screen / Esc	
Printer-friendly Version	
Interactive Discussion	

Africa, and contributions from the boreal Northern Hemisphere are also noticeable (not shown). We therefore deduce that the optimization of C_3 grasslands parameters is the most influential factor explaining the improved simulation of C_{CO_2} at this station, but also that the influence of boreal needleleaf evergreen forests cannot be neglected here.

5 The reduction of the simulated cycle amplitude is too strong at station Mauna Loa, which, combined with earlier seasonality, leads to a poorer model–data fit after optimization. The remote location of Mauna Loa (north Pacific) is sensitive to influences from most of the Northern Hemisphere. We find that the main drivers of the simulated correction are flattened, earlier C_{CO_2} variations in temperate and boreal regions 10 of North America and Asia, and Europe (not shown). These results thus reflect part of the reduction of the seasonal amplitude of NEE in boreal ecosystems and C_3 grasslands noticed at Alert and South Pole stations. The degraded model–data fit between optimized C_{CO_2} and data from Mauna Loa also suggests that the boreal correction of NEE amplitude is too strong or insufficiently compensated at large scale by the amplification 15 of the seasonal cycle at temperate latitudes visible at TempENF and TempDBF sites (see Sect. 3.1 and Fig. 3).

Finally, the optimized model overall brings a small improvement of the modeled interannual variability of C_{CO_2} , with a median reduction of 3.9 % for the RMSD between modeled and measured monthly anomaly (see Sect. 2.4). Forty-five locations, out of 20 the 53 used in this study, display an improvement, while at the remaining 8 sites the degradation of the simulated interannual variability remains small with RMSD increases always smaller than 1.5 %. These results suggest that despite the relative shortness (one to three years) of most of the FluxNet datasets selected to optimize the OR-CHIDEE model, the diversity of the covered weather situations gives a modest, yet 25 consistent source of information to better reproduce interannual variations of carbon fluxes at the global scale.



3.5.2 Global scale phenology index

Table 3 reports the median values of the correlation factor between weekly values of measured NDVI and modeled FAPAR during the period 2000–2010 (see Sect. 2.4), for each optimized PFT as well as over all the boxes used for calculation (including all 12

- 5 vegetated PFTs of ORCHIDEE), for both the prior and optimized model. There is no result for BorDBF whose vegetation fraction here never exceeds 40 %. All other PFTs exhibit a higher median correlation factor after optimization, which means the modeled leaf seasonal cycle better matches the global scale observations. This result is related to the improvement of the simulated GPP at FluxNet sites, the latter being partly driven
10 by the improvement of the seasonal variations of simulated LAI. The dominant feature seems to be a shorter growing season length for TempDBF, which is consistent with the site-level simulations of GPP seasonality for this PFT (Fig. 5), and an earlier beginning of the growing season for C₃ grasses (not shown). Note that this improvement also explains most of the increased correlation factor in temperate and boreal evergreen
15 forests. Indeed, the current formulation of the ORCHIDEE model makes deciduous and herbaceous PFTs the only significant contributors to the seasonal cycle at such a coarse resolution, even when these ecosystems are secondary and/or the understory within an evergreen-dominated forest. Lastly, the score for TropEBF remains poor because the model wrongly simulates the leaf renewal and the hydric stress during the
20 dry season, as discussed in Sects. 3.1 and 3.4.

4 Conclusion

Generalizing the results of Kuppel et al. (2012) across ecosystems, this study has shown that a significant degree of improvement is introduced to the simulation of carbon and water fluxes, through a generic optimization approach with in situ measurements of NEE and LE fluxes, relying on the traditional PFT classification used in many
25 land surface models. At the global scale, this optimization method allows first a better

Generic model optimization across ecosystems

S. Kuppel et al.

[Title Page](#)

[Abstract](#)

[Introduction](#)

[Conclusions](#)

[References](#)

[Tables](#)

[Figures](#)

◀

▶

◀

▶

[Back](#)

[Close](#)

[Full Screen / Esc](#)

[Printer-friendly Version](#)

[Interactive Discussion](#)



Title Page	
Abstract	Introduction
Conclusions	References
Tables	Figures
◀	▶
◀	▶
Back	Close
Full Screen / Esc	
Printer-friendly Version	
Interactive Discussion	



simulation of the seasonal foliar cover. Second, the multi-site parameter set has a significant leverage upon the simulated seasonality of atmospheric C_{CO_2} , with performances somewhat spatially heterogeneous and depending on the PFT considered, while a small, yet encouraging improvement of the simulated interannuality of C_{CO_2}

is found. The remaining discrepancies in C_{CO_2} indicate that combining atmospheric CO₂ concentration and a larger number of flux towers observations, in a Carbon Cycle multi-Data Assimilation Systems (CCDASs, e.g., Kaminski et al., 2013), would be beneficial. More generally, we suggest that the assimilation of FluxNet data should be considered as a baseline for the development of multi-data assimilation systems where more complementary data streams are combined. In particular, daytime and nighttime NEE could replace the daily values used here, and adding measurements of leaf area index, soil respiration fluxes (e.g. chamber measurements), biomass and litter/soil carbon pools, would help better separating the processes and constraining environmental drivers, as would a simultaneous parameter optimization of both over- and understory PFT fractions. Furthermore, the FluxNet multi-site approach could be used to characterize the structural, parametric and total uncertainties associated with the simulated annual biospheric carbon balance at regional-to-global scales, and to compare it with (1) the discrepancies of results between global ecosystem models (Sitch et al., 2008), and (2) the error carried by the terrestrial carbon fluxes estimated via inverse modeling with atmospheric transport models (e.g., Chevallier et al., 2010). The long-term problem is thus to evaluate what would be gained from simultaneously assimilating various data streams covering different spatial and temporal scales into a terrestrial ecosystem model, and how the PFT classification should be refined to maximize this improvement.

Code availability

The source code of the data assimilation system is available at <https://pypi.python.org/pypi/ORCHISM>. Regarding the ORCHIDEE vegetation model, the source files of the Tag version 1.9.5.2 used for this study can be obtained upon request (see

Title Page	
Abstract	Introduction
Conclusions	References
Tables	Figures
◀	▶
◀	▶
Back	Close
Full Screen / Esc	
Printer-friendly Version	
Interactive Discussion	



http://labex.ipsl.fr/orchidee/index.php/contact), while the associated documentation can be found at <https://forge.ipsl.jussieu.fr/orchidee/wiki/Documentation>. Note that the tangent linear version of the ORCHIDEE model has been generated using a commercial software (TAF, see Sect. 2.2). For this reason, only the “forward” version of the ORCHIDEE model is available for sharing, suitable for the finite differences method. Finally, the source code of the LMDz atmospheric transport model can be found at <http://web.lmd.jussieu.fr/trac>.

Supplementary material related to this article is available online at
[http://www.geosci-model-dev-discuss.net/7/2961/2014/
gmdd-7-2961-2014-supplement.pdf](http://www.geosci-model-dev-discuss.net/7/2961/2014/gmdd-7-2961-2014-supplement.pdf).

Acknowledgements. This work has been supported by the CARBONES project, within the EU’s 7th Framework Program for Research and Development. E. Vangorsel, J. Beringer, H. R. da Rocha, J. Grace, B. Kruijt, M. Goulden, A. Black, L. Flanagan, B. Amiro, J. H. McCaughey, H. Margolis, A. Barr, A. Arain, T. Kato, T. Foken, A. Knohl, A. Don, C. Rebmann, M.-J. Sanz, M. T. Sebastiá, T. Vesala, T. Laurila, E. Dufrêne, A. Granier, D. Loustau, N. Zoltan, T. Hirano, R. Valentini, D. Gianelle, A. Raschi, H. Kondo, A. J. Dolman, T. Johansson, M. Nilsson, A. Lindroth, A. Grelle, J. Moncrieff, M. Wilkinson, M. Torn, T. Meyers, A.D. Richardson, J. Randers, J. W. Munger, D. Hollinger, R. Matamala, W. C. Oechel, J. Hadley, B. Law, L. Gu, A. Noormets, P. Blanken, G. Bohrer, D. D. Baldocchi, P. Bolstad, and K. Bible are warmly thanked for making their flux measurements available. So are M. Grünwald and E. J. Moors for their useful comments on the manuscript, and G. Lasslop, M. Forkel, N. Carvalhais and M. Reichstein for applying the energy-balance corrections to the processed data. We are grateful to C. Bacour for the help while developing the optimization and the useful comments on the manuscript, to N. MacBean for setting up the global simulations, and to N. Viovy for the general discussions on the ORCHIDEE model. Finally, we would like to thank the computer team at LSCE for the computational resources provided.

References

Generic model optimization across ecosystems

S. Kuppel et al.

[Title Page](#)

[Abstract](#)

[Introduction](#)

[Conclusions](#)

[References](#)

[Tables](#)

[Figures](#)

[◀](#)

[▶](#)

[◀](#)

[▶](#)

[Back](#)

[Close](#)

[Full Screen / Esc](#)

[Printer-friendly Version](#)

[Interactive Discussion](#)



Title Page	
Abstract	Introduction
Conclusions	References
Tables	Figures
◀	▶
◀	▶
Back	Close
Full Screen / Esc	
Printer-friendly Version	
Interactive Discussion	



- Botta, A., Viovy, N., Ciais, P., Friedlingstein, P., and Monfray, P.: A global prognostic scheme of leaf onset using satellite data, *Glob. Change Biol.*, 6, 709–725, 2000.
- Braswell, B. H., Sacks, W. J., Linder, E., and Schimel, D. S.: Estimating diurnal to annual ecosystem parameters by synthesis of a carbon flux model with eddy covariance net ecosystem exchange observations, *Glob. Change Biol.*, 11, 335–355, doi:10.1111/j.1365-2486.2005.00897.x, 2005.
- Byrd, R. H., Lu, P., Nocedal, J., and Zhu, C.: A limited memory algorithm for bound constrained optimization, *SIAM J. Sci. Comput.*, 16, 1190–1208, doi:10.1137/0916069, 1995.
- Carswell, F. E., Costa, A. L., Palheta, M., Malhi, Y., Meir, P., de Costa, J. P. R., de Ruivo, M. L., do Leal, L. S. M., Costa, J. M. N., Clement, R. J., and Grace, J.: Seasonality in CO₂ and H₂O flux at an eastern Amazonian rain forest, *J. Geophys. Res.-Atmos.*, 107, 43-1–43-16, doi:10.1029/2000JD000284, 2002.
- Carvalhais, N., Reichstein, M., Ciais, P., Collatz, G. J., Mahecha, M. D., Montagnani, L., Paepale, D., Rambal, S., and Seixas, J.: Identification of vegetation and soil carbon pools out of equilibrium in a process model via eddy covariance and biometric constraints, *Glob. Change Biol.*, 16, 2813–2829, doi:10.1111/j.1365-2486.2010.02173.x, 2010.
- Chave, J., Navarrete, D., Almeida, S., Álvarez, E., Aragão, L. E. O. C., Bonal, D., Châtelet, P., Silva-Espejo, J. E., Goret, J.-Y., von Hildebrand, P., Jiménez, E., Patiño, S., Peñuela, M. C., Phillips, O. L., Stevenson, P., and Malhi, Y.: Regional and seasonal patterns of litterfall in tropical South America, *Biogeosciences*, 7, 43–55, doi:10.5194/bg-7-43-2010, 2010.
- Chevallier, F., Ciais, P., Conway, T. J., Aalto, T., Anderson, B. E., Bousquet, P., Brunke, E. G., Ciattaglia, L., Esaki, Y., Fröhlich, M., Gomez, A., Gomez-Pelaez, A. J., Haszpra, L., Krummel, P. B., Langenfelds, R. L., Leuenberger, M., Machida, T., Maignan, F., Matsueda, H., Morguí, J. A., Mukai, H., Nakazawa, T., Peylin, P., Ramonet, M., Rivier, L., Sawa, Y., Schmidt, M., Steele, L. P., Vay, S. A., Vermeulen, A. T., Wofsy, S., and Worthy, D.: CO₂ surface fluxes at grid point scale estimated from a global 21 year reanalysis of atmospheric measurements, *J. Geophys. Res.*, 115, D21307, doi:10.1029/2010JD013887, 2010.
- Chiesi, M., Maselli, F., Bindi, M., Fibbi, L., Cherubini, P., Arlotta, E., Tirone, G., Matteucci, G., and Seufert, G.: Modelling carbon budget of Mediterranean forests using ground and remote sensing measurements, *Agr. Forest Meteorol.*, 135, 22–34, doi:10.1016/j.agrformet.2005.09.011, 2005.
- Christensen, T. R., Johansson, T., Olsrud, M., Ström, L., Lindroth, A., Masteponov, M., Malmer, N., Friberg, T., Crill, P., and Callaghan, T. V.: A catchment-scale carbon and

Generic model optimization across ecosystems

S. Kuppel et al.

[Title Page](#)

[Abstract](#)

[Introduction](#)

[Conclusions](#)

[References](#)

[Tables](#)

[Figures](#)

◀

▶

◀

▶

[Back](#)

[Close](#)

[Full Screen / Esc](#)

[Printer-friendly Version](#)

[Interactive Discussion](#)



Dolman, A. J., Moors, E. J., and Elbers, J. A.: The carbon uptake of a mid latitude pine forest growing on sandy soil, *Agr. Forest Meteorol.*, 111, 157–170, doi:10.1016/S0168-1923(02)00024-2, 2002.

Don, A., Rebmann, C., Kolle, O., Scherer-Lorenzen, M., and Schulze, E.-D.: Impact of afforestation-associated management changes on the carbon balance of grassland, *Glob. Change Biol.*, 15, 1990–2002, doi:10.1111/j.1365-2486.2009.01873.x, 2009.

Ducoudré, N. I., Laval, K., and Perrier, A.: SECHIBA, a new set of parameterizations of the hydrologic exchanges at the land–atmosphere interface within the LMD Atmospheric General Circulation Model, *J. Climate*, 6, 248–273, doi:10.1175/1520-0442(1993)006<0248:SANSOP>2.0.CO;2, 1993.

Dunn, A. L., Barford, C. C., Wofsy, S. C., Goulden, M. L., and Daube, B. C.: A long-term record of carbon exchange in a boreal black spruce forest: means, responses to interannual variability, and decadal trends, *Glob. Change Biol.*, 13, 577–590, doi:10.1111/j.1365-2486.2006.01221.x, 2007.

Eidenshink, J. C. and Faundeen, J. L.: The 1 km AVHRR global land data set: first stages in implementation, *Int. J. Remote Sens.*, 15, 3443–3462, doi:10.1080/01431169408954339, 1994.

Falk, M., Wharton, S., Schroeder, M., Ustin, S., and U, K. T. P.: Flux partitioning in an old-growth forest: seasonal and interannual dynamics, *Tree Physiol.*, 28, 509–520, doi:10.1093/treephys/28.4.509, 2008.

Fischer, M. L., Billesbach, D. P., Berry, J. A., Riley, W. J., and Torn, M. S.: Spatiotemporal variations in growing season exchanges of CO₂, H₂O, and sensible heat in agricultural fields of the Southern Great Plains, *Earth Interact.*, 11, 1–21, doi:10.1175/EI231.1, 2007.

Flanagan, L. B. and Adkinson, A. C.: Interacting controls on productivity in a northern Great Plains grassland and implications for response to ENSO events: controls on grassland productivity, *Glob. Change Biol.*, 17, 3293–3311, doi:10.1111/j.1365-2486.2011.02461.x, 2011.

Friedlingstein, P., Cox, P., Betts, R., Bopp, L., von Bloh, W., Brovkin, V., Cadule, P., Doney, S., Eby, M., Fung, I., Bala, G., John, J., Jones, C., Joos, F., Kato, T., Kawamiya, M., Knorr, W., Lindsay, K., Matthews, H. D., Raddatz, T., Rayner, P., Reick, C., Roeckner, E., Schnitzler, K.-G., Schnur, R., Strassmann, K., Weaver, A. J., Yoshikawa, C., and Zeng, N.: Climate–Carbon Cycle Feedback Analysis: results from the C⁴MIP Model Intercomparison, *J. Climate*, 19, 3337–3353, doi:10.1175/JCLI3800.1, 2006.

Generic model optimization across ecosystems**S. Kuppel et al.**[Title Page](#)[Abstract](#)[Introduction](#)[Conclusions](#)[References](#)[Tables](#)[Figures](#)[Back](#)[Close](#)[Full Screen / Esc](#)[Printer-friendly Version](#)[Interactive Discussion](#)

Generic model optimization across ecosystems

S. Kuppel et al.

[Title Page](#)

[Abstract](#)

[Introduction](#)

[Conclusions](#)

[References](#)

[Tables](#)

[Figures](#)

◀

▶

◀

▶

[Back](#)

[Close](#)

[Full Screen / Esc](#)

[Printer-friendly Version](#)

[Interactive Discussion](#)



Garrigues, S., Lacaze, R., Baret, F., Morisette, J. T., Weiss, M., Nickeson, J. E., Fernandes, R., Plummer, S., Shabanov, N. V., Myneni, R. B., Knyazikhin, Y., and Yang, W.: Validation and intercomparison of global Leaf Area Index products derived from remote sensing data, *J. Geophys. Res.-Biogeo.*, 113, G02028, doi:10.1029/2007JG000635, 2008.

5 Gianelle, D., Vescovo, L., Marcolla, B., Manca, G., and Cescatti, A.: Ecosystem carbon fluxes and canopy spectral reflectance of a mountain meadow, *Int. J. Remote Sens.*, 30, 435–449, doi:10.1080/01431160802314855, 2009.

Giering, R., Kaminski, T., and Slawig, T.: Generating efficient derivative code with TAF: adjoint and tangent linear Euler flow around an airfoil, *Future Gener. Comp. Sy.*, 21, 1345–1355, doi:10.1016/j.future.2004.11.003, 2005.

10 Gilmanov, T. G., Tieszen, L. L., Wylie, B. K., Flanagan, L. B., Frank, A. B., Haferkamp, M. R., Meyers, T. P., and Morgan, J. A.: Integration of CO₂ flux and remotely-sensed data for primary production and ecosystem respiration analyses in the Northern Great Plains: potential for quantitative spatial extrapolation, *Global Ecol. Biogeogr.*, 14, 271–292, doi:10.1111/j.1466-822X.2005.00151.x, 2005.

15 Gilmanov, T. G., Soussana, J. F., Aires, L., Allard, V., Ammann, C., Balzarolo, M., Barcza, Z., Bernhofer, C., Campbell, C. L., Cernusca, A., Cescatti, A., Clifton-Brown, J., Dirks, B. O. M., Dore, S., Eugster, W., Fuhrer, J., Gimeno, C., Gruenwald, T., Haszpra, L., Hensen, A., Ibrom, A., Jacobs, A. F. G., Jones, M. B., Lanigan, G., Laurila, T., Lohila, A., Manca, Marcolla, B., Nagy, Z., Pilegaard, K., Pinter, K., Pio, C., Raschi, A., Rogiers, N., Sanz, M. J., Stefani, P., Sutton, M., Tuba, Z., Valentini, R., Williams, M. L., and Wohlfahrt, G.: Partitioning European grassland net ecosystem CO₂ exchange into gross primary productivity and ecosystem respiration using light response function analysis, *Agr. Ecosyst. Environ.*, 121, 93–120, doi:10.1016/j.agee.2006.12.008, 2007.

20 Gioli, B., Miglietta, F., De Martino, B., Hutjes, R. W. A., Dolman, H. A. J., Lindroth, A., Schumacher, M., Sanz, M. J., Manca, G., Peressotti, A., and Dumas, E. J.: Comparison between tower and aircraft-based eddy covariance fluxes in five European regions, *Agr. Forest Meteorol.*, 127, 1–16, doi:10.1016/j.agrformet.2004.08.004, 2004.

25 GLOBALVIEW-CO₂: Cooperative Global Atmospheric Data Integration Project. Multi-laboratory compilation of synchronized and gap-filled atmospheric carbon dioxide records for the period 1979–2012 (obspack_co2_1_GLOBALVIEW-CO₂_2013_v1.0.4_2013-12-23), Compiled by NOAA Global Monitoring Division: Boulder, Colorado, USA Data product accessed at doi:10.3334/OBSPACK/1002, updated annually, 2013.

[Title Page](#)
[Abstract](#) [Introduction](#)
[Conclusions](#) [References](#)
[Tables](#) [Figures](#)
[◀](#) [▶](#)
[◀](#) [▶](#)
[Back](#) [Close](#)
[Full Screen / Esc](#)
[Printer-friendly Version](#)
[Interactive Discussion](#)

Goulden, M. L., Miller, S. D., da Rocha, H. R., Menton, M. C., de Freitas, H. C., e Silva Figueira, A. M., and de Sousa, C. A. D.: Diel and seasonal patterns of tropical forest CO₂ exchange, *Ecol. Appl.*, 14, 42–54, doi:10.1890/02-6008, 2004.

Goulden, M. L., Winston, G. C., McMillan, A. M. S., Litvak, M. E., Read, E. L., Rocha, A. V., and Rob Elliot, J.: An eddy covariance mesonet to measure the effect of forest age on land–atmosphere exchange, *Glob. Change Biol.*, 12, 2146–2162, doi:10.1111/j.1365-2486.2006.01251.x, 2006.

Granier, A., Bréda, N., Longdoz, B., Gross, P., and Ngao, J.: Ten years of fluxes and stand growth in a young beech forest at Hesse, North-eastern France, *Ann. For. Sci.*, 65, 704–716, doi:10.1051/forest:2008052, 2008.

Groenendijk, M., Dolman, A. J., van der Molen, M. K., Leuning, R., Arneth, A., Delpierre, N., Gash, J. H. C., Lindroth, A., Richardson, A. D., Verbeeck, H., and Wohlfahrt, G.: Assessing parameter variability in a photosynthesis model within and between plant functional types using global Fluxnet eddy covariance data, *Agr. Forest Meteorol.*, 151, 22–38, doi:10.1016/j.agrformet.2010.08.013, 2011.

Grünwald, T. and Bernhofer, C.: A decade of carbon, water and energy flux measurements of an old spruce forest at the Anchor Station Tharandt, *Tellus B*, 59, 387–396, doi:10.1111/j.1600-0889.2007.00259.x, 2007.

Gu, L., Massman, W. J., Leuning, R., Pallardy, S. G., Meyers, T., Hanson, P. J., Riggs, J. S., Hosman, K. P., and Yang, B.: The fundamental equation of eddy covariance and its application in flux measurements, *Agr. Forest Meteorol.*, 152, 135–148, doi:10.1016/j.agrformet.2011.09.014, 2012.

Gurney, K. R., Law, R. M., Denning, A. S., Rayner, P. J., Baker, D., Bousquet, P., Bruhwiler, L., Chen, Y.-H., Ciais, P., Fan, S., Fung, I. Y., Gloor, M., Heimann, M., Higuchi, K., John, J., Kowalczyk, E., Maki, T., Maksyutov, S., Peylin, P., Prather, M., Pak, B. C., Sarmiento, J., Taguchi, S., Takahashi, T., and Yuen, C.-W.: TransCom 3 CO₂ inversion intercomparison: 1. Annual mean control results and sensitivity to transport and prior flux information, *Tellus B*, 55, 555–579, doi:10.1034/j.1600-0889.2003.00049.x, 2003.

Hadley, J. L., Kuzeja, P. S., Daley, M. J., Phillips, N. G., Mulcahy, T., and Singh, S.: Water use and carbon exchange of red oak- and eastern hemlock-dominated forests in the northeastern USA: implications for ecosystem-level effects of hemlock woolly adelgid, *Tree Physiol.*, 28, 615–627, doi:10.1093/treephys/28.4.615, 2008.



Hendriks, D. M. D., van Huissteden, J., Dolman, A. J., and van der Molen, M. K.: The full greenhouse gas balance of an abandoned peat meadow, *Biogeosciences*, 4, 411–424, doi:10.5194/bg-4-411-2007, 2007.

Hirano, T., Segah, H., Harada, T., Limin, S., June, T., Hirata, R., and Osaki, M.: Carbon dioxide balance of a tropical peat swamp forest in Kalimantan, Indonesia, *Glob. Change Biol.*, 13, 412–425, doi:10.1111/j.1365-2486.2006.01301.x, 2007.

Hollinger, D. Y., Aber, J., Dail, B., Davidson, E. A., Goltz, S. M., Hughes, H., Leclerc, M. Y., Lee, J. T., Richardson, A. D., Rodrigues, C., Scott, N. a., Achuatavarier, D., and Walsh, J.: Spatial and temporal variability in forest–atmosphere CO₂ exchange, *Glob. Change Biol.*, 10, 1689–1706, doi:10.1111/j.1365-2486.2004.00847.x, 2004.

Hourdin, F., Musat, I., Bony, S., Braconnot, P., Codron, F., Dufresne, J.-L., Fairhead, L., Filiberti, M.-A., Friedlingstein, P., Grandpeix, J.-Y., Krinner, G., LeVan, P., Li, Z.-X., and Lott, F.: The LMDZ4 general circulation model: climate performance and sensitivity to parametrized physics with emphasis on tropical convection, *Clim. Dynam.*, 27, 787–813, doi:10.1007/s00382-006-0158-0, 2006.

Howard, E. A., Gower, S. T., Foley, J. A., and Kucharik, C. J.: Effects of logging on carbon dynamics of a jack pine forest in Saskatchewan, Canada, *Glob. Change Biol.*, 10, 1267–1284, doi:10.1111/j.1529-8817.2003.00804.x, 2004.

Ito, A., Muraoka, H., Koizumi, H., Saigusa, N., Murayama, S., and Yamamoto, S.: Seasonal variation in leaf properties and ecosystem carbon budget in a cool-temperate deciduous broad-leaved forest: simulation analysis at Takayama site, Japan, *Ecol. Res.*, 21, 137–149, doi:10.1007/s11284-005-0100-7, 2006.

Jacobs, C. M. J., Jacobs, A. F. G., Bosveld, F. C., Hendriks, D. M. D., Hensen, A., Kroon, P. S., Moors, E. J., Nol, L., Schrier-Uijl, A., and Veenendaal, E. M.: Variability of annual CO₂ exchange from Dutch grasslands, *Biogeosciences*, 4, 803–816, doi:10.5194/bg-4-803-2007, 2007.

Jarvis, P. G.: Scaling processes and problems, *Plant Cell Environ.*, 18, 1079–1089, doi:10.1111/j.1365-3040.1995.tb00620.x, 1995.

Jassal, R. S., Black, T. A., Novak, M. D., Gaumont-Guay, D., and Nesic, Z.: Effect of soil water stress on soil respiration and its temperature sensitivity in an 18-year-old temperate Douglas-fir stand, *Glob. Change Biol.*, 14, 1305–1318, doi:10.1111/j.1365-2486.2008.01573.x, 2008.

Jenkins, J. P., Richardson, A. D., Braswell, B. H., Ollinger, S. V., Hollinger, D. Y., and Smith, M.-L.: Refining light-use efficiency calculations for a deciduous forest canopy using simultaneous

Generic model optimization across ecosystems

S. Kuppel et al.

[Title Page](#)

[Abstract](#)

[Introduction](#)

[Conclusions](#)

[References](#)

[Tables](#)

[Figures](#)

◀

▶

◀

▶

[Back](#)

[Close](#)

[Full Screen / Esc](#)

[Printer-friendly Version](#)

[Interactive Discussion](#)



- 10 Kato, T., Tang, Y., Gu, S., Hirota, M., Du, M., Li, Y., and Zhao, X.: Temperature and biomass influences on interannual changes in CO₂ exchange in an alpine meadow on the Qinghai-Tibetan Plateau, *Glob. Change Biol.*, 12, 1285–1298, doi:10.1111/j.1365-2486.2006.01153.x, 2006.

15 Kattege, J., Díaz, S., Lavorel, S., Prentice, I. C., Leadley, P., Bönisch, G., Garnier, E., Westoby, M., Reich, P. B., Wright, I. J., Cornelissen, J. H. C., Violle, C., Harrison, S. P., Van Bodegom, P. M., Reichstein, M., Enquist, B. J., Soudzilovskaia, N. A., Ackerly, D. D., Anand, M., Atkin, O., Bahn, M., Baker, T. R., Baldocchi, D., Bekker, R., Blanco, C. C., Blonder, B., Bond, W. J., Bradstock, R., Bunker, D. E., Casanoves, F., Cavender-Bares, J., Chambers, J. Q., Chapin III, F. S., Chave, J., Coomes, D., Cornwell, W. K., Craine, J. M., Dobrin, B. H., Duarte, L., Durka, W., Elser, J., Esser, G., Estiarte, M., Fagan, W. F., Fang, J., Fernández-Méndez, F., Fidelis, A., Finegan, B., Flores, O., Ford, H., Frank, D., Freschet, G. T., Fyllas, N. M., Gallagher, R. V., Green, W. A., Gutierrez, A. G., Hickler, T., Higgins, S. I., Hodgson, J. G., Jalili, A., Jansen, S., Joly, C. A., Kerkhoff, A. J., Kirkup, D., Kitajima, K., Kleyer, M., Klotz, S., Knops, J. M. H., Kramer, K., Kühn, I., Kurokawa, H., Laughlin, D., Lee, T. D., Leishman, M., Lens, F., Lenz, T., Lewis, S. L., Lloyd, J., Llusià, J., Louault, F., Ma, S., Mahecha, M. D., Manning, P., Massad, T., Medlyn, B. E., Messier, J., Moles, A. T., Müller, S. C., Nadrowski, K., Naeem, S., Niinemets, Ü., Nöllert, S., Nüske, A., Ogaya, R., Oleksyn, J., Onipchenko, V. G., Onoda, Y., OrdoñEZ, J., Overbeck, G. et al.: TRY – a global database of plant traits, *Glob. Change Biol.*, 17, 2905–2935, doi:10.1111/j.1365-2486.2011.02451.x, 2011.

20 25 30 Keenan, T. F., Davidson, E., Moffat, A. M., Munger, W., and Richardson, A. D.: Using model-data fusion to interpret past trends, and quantify uncertainties in future projections, of terrestrial ecosystem carbon cycling, *Glob. Change Biol.*, 18, 2555–2569, doi:10.1111/j.1365-2486.2012.02684.x, 2012.

Generic model optimization across ecosystems

S. Kuppel et al.

Title Page

Abstract

Introduction

Conclusion:

References

Tables

Figures



Back

Close

Full Screen / Esc

[Printer-friendly Version](#)

Interactive Discussion



Generic model optimization across ecosystems**S. Kuppel et al.**[Title Page](#)[Abstract](#)[Introduction](#)[Conclusions](#)[References](#)[Tables](#)[Figures](#)[◀](#)[▶](#)[◀](#)[▶](#)[Back](#)[Close](#)[Full Screen / Esc](#)[Printer-friendly Version](#)[Interactive Discussion](#)

Kilinc, M., Beringer, J., Hutley, L. B., Tapper, N. J., and McGuire, D. A.: Carbon and water exchange of the world's tallest angiosperm forest, *Agr. Forest Meteorol.*, 182–183, 215–224, doi:10.1016/j.agrformet.2013.07.003, 2013.

Knorr, W. and Kattge, J.: Inversion of terrestrial ecosystem model parameter values against eddy covariance measurements by Monte Carlo sampling, *Glob. Change Biol.*, 11, 1333–1351, doi:10.1111/j.1365-2486.2005.00977.x, 2005.

Krinner, G., Viovy, N., de Noblet-Ducoudré, N., Ogée, J., Polcher, J., Friedlingstein, P., Ciais, P., Sitch, S., and Prentice, I. C.: A dynamic global vegetation model for studies of the coupled atmosphere-biosphere system, *Global Biogeochem. Cy.*, 19, GB1015, doi:10.1029/2003GB002199, 2005.

Krishnan, P., Black, T. A., Barr, A. G., Grant, N. J., Gaumont-Guay, D., and Nesic, Z.: Factors controlling the interannual variability in the carbon balance of a southern boreal black spruce forest, *J. Geophys. Res.-Atmos.*, 113, D09109, doi:10.1029/2007JD008965, 2008.

Kuppel, S., Peylin, P., Chevallier, F., Bacour, C., Maignan, F., and Richardson, A. D.: Constraining a global ecosystem model with multi-site eddy-covariance data, *Biogeosciences*, 9, 3757–3776, doi:10.5194/bg-9-3757-2012, 2012.

Kuppel, S., Chevallier, F., and Peylin, P.: Quantifying the model structural error in carbon cycle data assimilation systems, *Geosci. Model Dev.*, 6, 45–55, doi:10.5194/gmd-6-45-2013, 2013.

Lagergren, F., Lindroth, A., Dellwik, E., Ibrom, A., Lankreijer, H., Launiainen, S., Mölder, M., Kolari, P., Pilegaard, K., and Vesala, T.: Biophysical controls on CO₂ fluxes of three Northern forests based on long-term eddy covariance data, *Tellus B*, 60, 143–152, doi:10.1111/j.1600-0889.2006.00324.x, 2008.

Lasslop, G., Reichstein, M., Kattge, J., and Papale, D.: Influences of observation errors in eddy flux data on inverse model parameter estimation, *Biogeosciences*, 5, 1311–1324, doi:10.5194/bg-5-1311-2008, 2008.

Leuning, R., Cleugh, H. A., Zegelin, S. J., and Hughes, D.: Carbon and water fluxes over a temperate Eucalyptus forest and a tropical wet/dry savanna in Australia: measurements and comparison with MODIS remote sensing estimates, *Agr. Forest Meteorol.*, 129, 151–173, doi:10.1016/j.agrformet.2004.12.004, 2005.

Lindroth, A., Klemedtsson, L., Grelle, A., Weslien, P., and Langvall, O.: Measurement of net ecosystem exchange, productivity and respiration in three spruce forests in Sweden shows

Generic model optimization across ecosystems

S. Kuppel et al.

[Title Page](#)

[Abstract](#)

[Introduction](#)

[Conclusions](#)

[References](#)

[Tables](#)

[Figures](#)

◀

▶

◀

▶

[Back](#)

[Close](#)

[Full Screen / Esc](#)

[Printer-friendly Version](#)

[Interactive Discussion](#)



Generic model optimization across ecosystems

S. Kuppel et al.

[Title Page](#)

[Abstract](#)

[Introduction](#)

[Conclusions](#)

[References](#)

[Tables](#)

[Figures](#)

◀

▶

[Back](#)

[Close](#)

[Full Screen / Esc](#)

[Printer-friendly Version](#)

[Interactive Discussion](#)



Mund, M., Kutsch, W. L., Wirth, C., Kahl, T., Knohl, A., Skomarkova, M. V., and Schulze, E.-D.: The influence of climate and fructification on the inter-annual variability of stem growth and net primary productivity in an old-growth, mixed beech forest, *Tree Physiol.*, 30, 689–704, doi:10.1093/treephys/tpq027, 2010.

5 Nagy, Z., Pintér, K., Czóbel, S., Balogh, J., Horváth, L., Fóti, S., Barcza, Z., Weidinger, T., Csintalan, Z., Dinh, N. Q., Grosz, B., and Tuba, Z.: The carbon budget of semi-arid grassland in a wet and a dry year in Hungary, *Agr. Ecosyst. Environ.*, 121, 21–29, doi:10.1016/j.agee.2006.12.003, 2007.

10 Nash, J. E. and Sutcliffe, J. V.: River flow forecasting through conceptual models part I – A discussion of principles, *J. Hydrol.*, 10, 282–290, doi:10.1016/0022-1694(70)90255-6, 1970.

Nave, L. E., Gough, C. M., Maurer, K. D., Bohrer, G., Hardiman, B. S., Le Moine, J., Munoz, A. B., Nadelhoffer, K. J., Sparks, J. P., Strahm, B. D., Vogel, C. S., and Curtis, P. S.: Disturbance and the resilience of coupled carbon and nitrogen cycling in a north temperate forest, *J. Geophys. Res.*, 116, G04016, doi:10.1029/2011JG001758, 2011.

15 Noormets, A., Gavazzi, M. J., Mcnulty, S. G., Domec, J.-C., Sun, G., King, J. S., and Chen, J.: Response of carbon fluxes to drought in a coastal plain loblolly pine forest, *Glob. Change Biol.*, 16, 272–287, doi:10.1111/j.1365-2486.2009.01928.x, 2010.

Oechel, W. C., Vourlitis, G. L., Hastings, S. J., Zulueta, R. C., Hinzman, L., and Kane, D.: Acclimation of ecosystem CO₂ exchange in the Alaskan Arctic in response to decadal climate warming, *Nature*, 406, 978–981, doi:10.1038/35023137, 2000.

20 Olson, J.: Global Ecosystem Framework-Definitions, USGS EROS Data Center, Internal Report, Sioux Falls, SD, 37, 1994.

Papale, D.: Towards a Standardized Processing of Net Ecosystem Exchange Measured with Eddy Covariance Technique: Algorithms and Uncertainty Estimation, available at: <http://dspace.unitus.it/handle/2067/1321> (last access: 27 August 2013), 2006.

25 Peichl, M., Leahy, P., and Kiely, G.: Six-year stable annual uptake of carbon dioxide in intensively managed humid temperate grassland, *Ecosystems*, 14, 112–126, doi:10.1007/s10021-010-9398-2, 2011.

Pintér, K., Barcza, Z., Balogh, J., Czóbel, S., Csintalan, Z., Tuba, Z., and Nagy, Z.: Interannual variability of grasslands' carbon balance depends on soil type, *Community Ecol.*, 9, 43–48, doi:10.1556/ComEc.9.2008.S.7, 2008.

30 Pitman, A. J.: The evolution of, and revolution in, land surface schemes designed for climate models, *Int. J. Climatol.*, 23, 479–510, doi:10.1002/joc.893, 2003.

Generic model optimization across ecosystems

S. Kuppel et al.

[Title Page](#)

[Abstract](#)

[Introduction](#)

[Conclusions](#)

[References](#)

[Tables](#)

[Figures](#)

◀

▶

◀

▶

[Back](#)

[Close](#)

[Full Screen / Esc](#)

[Printer-friendly Version](#)

[Interactive Discussion](#)



Raupach, M. R., Rayner, P. J., Barrett, D. J., DeFries, R. S., Heimann, M., Ojima, D. S., Quegan, S., and Schmullius, C. C.: Model–data synthesis in terrestrial carbon observation: methods, data requirements and data uncertainty specifications, *Glob. Change Biol.*, 11, 378–397, doi:10.1111/j.1365-2486.2005.00917.x, 2005.

Rebmann, C., Zeri, M., Lasslop, G., Mund, M., Kolle, O., Schulze, E.-D., and Feigenwinter, C.: Treatment and assessment of the CO₂-exchange at a complex forest site in Thuringia, Germany, *Agr. Forest Meteorol.*, 150, 684–691, doi:10.1016/j.agrformet.2009.11.001, 2010.

Reichstein, M., Tenhunen, J., Roupsard, O., Ourcival, J.-M., Rambal, S., Miglietta, F., Peressotti, A., Pecchiari, M., Tirone, G., and Valentini, R.: Inverse modeling of seasonal drought effects on canopy CO₂/H₂O exchange in three Mediterranean ecosystems, *J. Geophys. Res.-Atmos.*, 108, D23472, doi:10.1029/2003JD003430, 2003.

Reichstein, M., Falge, E., Baldocchi, D., Papale, D., Aubinet, M., Berbigier, P., Bernhofer, C., Buchmann, N., Gilmanov, T., Granier, A., Grunwald, T., Havrankova, K., Ilvesniemi, H., Janous, D., Knohl, A., Laurila, T., Lohila, A., Loustau, D., Matteucci, G., Meyers, T., Miglietta, F., Ourcival, J.-M., Pumpanen, J., Rambal, S., Rotenberg, E., Sanz, M., Tenhunen, J., Seufert, G., Vaccari, F., Vesala, T., Yakir, D., and Valentini, R.: On the separation of net ecosystem exchange into assimilation and ecosystem respiration: review and improved algorithm, *Glob. Change Biol.*, 11, 1424–1439, doi:10.1111/j.1365-2486.2005.001002.x, 2005.

Richardson, A. D., Mahecha, M. D., Falge, E., Kattge, J., Moffat, A. M., Papale, D., Reichstein, M., Stauch, V. J., Braswell, B. H., Churkina, G., Kruijt, B., and Hollinger, D. Y.: Statistical properties of random CO₂ flux measurement uncertainty inferred from model residuals, *Agr. Forest Meteorol.*, 148, 38–50, doi:10.1016/j.agrformet.2007.09.001, 2008.

Sacks, W. J., Schimel, D. S., Monson, R. K., and Braswell, B. H.: Model–data synthesis of diurnal and seasonal CO₂ fluxes at Niwot Ridge, Colorado, *Glob. Change Biol.*, 12, 240–259, doi:10.1111/j.1365-2486.2005.01059.x, 2006.

Sagerfors, J., Lindroth, A., Grelle, A., Klemedtsson, L., Weslien, P., and Nilsson, M.: Annual CO₂ exchange between a nutrient-poor, minerotrophic, boreal mire and the atmosphere, *J. Geophys. Res.-Biogeo.*, 113, G01001, doi:10.1029/2006JG000306, 2008.

Sánchez, J. M., Caselles, V., Niclòs, R., Coll, C., and Kustas, W. P.: Estimating energy balance fluxes above a boreal forest from radiometric temperature observations, *Agr. Forest Meteorol.*, 149, 1037–1049, doi:10.1016/j.agrformet.2008.12.009, 2009.

Santaren, D., Peylin, P., Bacour, C., Ciais, P., and Longdoz, B.: Ecosystem model optimization using in-situ flux observations: benefit of monte-carlo vs. variational schemes and analy-

Generic model optimization across ecosystems

S. Kuppel et al.

[Title Page](#)

[Abstract](#)

[Introduction](#)

[Conclusions](#)

[References](#)

[Tables](#)

[Figures](#)

◀

▶

◀

▶

[Back](#)

[Close](#)

[Full Screen / Esc](#)

[Printer-friendly Version](#)

[Interactive Discussion](#)



- ses of the year-to-year model performances, *Biogeosciences Discuss.*, 10, 18009–18064, doi:10.5194/bgd-10-18009-2013, 2013.
- 5 Santaren, D., Peylin, P., Viovy, N., and Ciais, P.: Optimizing a process-based ecosystem model with eddy-covariance flux measurements: a pine forest in southern France, *Global Biogeochem. Cy.*, 21, GB2013, doi:10.1029/2006GB002834, 2007.
- Sellers, P. J., Randall, D. A., Collatz, G. J., Berry, J. A., Field, C. B., Dazlich, D. A., Zhang, C., Collelo, G. D., and Bounoua, L.: A revised land surface parameterization (SiB2) for atmospheric GCMS. Part I: Model formulation, *J. Climate*, 9, 676–705, doi:10.1175/1520-0442(1996)009<0676:ARLSPF>2.0.CO;2, 1996.
- 10 Sitch, S., Huntingford, C., Gedney, N., Levy, P. E., Lomas, M., Piao, S. L., Betts, R., Ciais, P., Cox, P., Friedlingstein, P., Jones, C. D., Prentice, I. C., and Woodward, F. I.: Evaluation of the terrestrial carbon cycle, future plant geography and climate-carbon cycle feedbacks using five Dynamic Global Vegetation Models (DGVMs), *Glob. Change Biol.*, 14, 2015–2039, doi:10.1111/j.1365-2486.2008.01626.x, 2008.
- 15 Staudt, K. and Foken, T.: Documentation of reference data for the experimental areas of the Bayreuth Centre for Ecology and Environmental Research (BayCEER) at the Waldstein site, *Arbeitsergebnisse Univ. Bayreuth Abt. Mikrometeorologie*, 35, available at: <http://d-nb.info/101053145X/34> (last access: 13 December 2013), 2007.
- 20 Suni, T., Rinne, J., Reissell, A., Altimir, N., Keronen, P., Rannik, Ü., Dal Maso, M., Kulmala, M., and Vesala, T.: Long-term measurements of surface fluxes above a Scots pine forest in Hyttiälä, southern Finland, 1996–2001, *Boreal Environ. Res.*, 8, 287–301, 2003.
- 25 Takahashi, T., Sutherland, S. C., Wanninkhof, R., Sweeney, C., Feely, R. A., Chipman, D. W., Hales, B., Friederich, G., Chavez, F., Sabine, C., Watson, A., Bakker, D. C. E., Schuster, U., Metzl, N., Yoshikawa-Inoue, H., Ishii, M., Midorikawa, T., Nojiri, Y., Kötzinger, A., Steinhoff, T., Hoppema, M., Olafsson, J., Arnarson, T. S., Tilbrook, B., Johannessen, T., Olsen, A., Bellerby, R., Wong, C. S., Delille, B., Bates, N. R., and de Baar, H. J. W.: Climatological mean and decadal change in surface ocean $p\text{CO}_2$, and net sea-air CO_2 flux over the global oceans, *Deep-Sea Res. Pt. II*, 56, 554–577, doi:10.1016/j.dsrr.2008.12.009, 2009.
- 30 Tarantola, A.: *Inverse Problem Theory and Methods for Model Parameter Estimation*, Society for Industrial and Applied Mathematics, Philadelphia, PA, 2005.
- Thoning, K. W., Tans, P. P., and Komhyr, W. D.: Atmospheric carbon dioxide at Mauna Loa Observatory: 2. Analysis of the NOAA GMCC data, 1974–1985, *J. Geophys. Res.-Atmos.*, 94, 8549–8565, doi:10.1029/JD094iD06p08549, 1989.

Generic model optimization across ecosystems

S. Kuppel et al.

[Title Page](#)

[Abstract](#)

[Introduction](#)

[Conclusions](#)

[References](#)

[Tables](#)

[Figures](#)

◀

▶

◀

▶

[Back](#)

[Close](#)

[Full Screen / Esc](#)

[Printer-friendly Version](#)

[Interactive Discussion](#)



Thum, T., Aalto, T., Laurila, T., Aurela, M., Lindroth, A., and Vesala, T.: Assessing seasonality of biochemical CO₂ exchange model parameters from micrometeorological flux observations at boreal coniferous forest, *Biogeosciences*, 5, 1625–1639, doi:10.5194/bg-5-1625-2008, 2008.

5 Twine, T. E., Kustas, W. P., Norman, J. M., Cook, D. R., Houser, P. R., Meyers, T. P., Prueger, J. H., Starks, P. J., and Wesely, M. L.: Correcting eddy-covariance flux underestimates over a grassland, *Agr. Forest Meteorol.*, 103, 279–300, doi:10.1016/S0168-1923(00)00123-4, 2000.

10 Urbanski, S., Barford, C., Wofsy, S., Kucharik, C., Pyle, E., Budney, J., McKain, K., Fitz-jarrald, D., Czikowsky, M., and Munger, J. W.: Factors controlling CO₂ exchange on timescales from hourly to decadal at Harvard Forest, *J. Geophys. Res.-Biogeo.*, 112, G02020, doi:10.1029/2006JG000293, 2007.

15 Verbeeck, H., Peylin, P., Bacour, C., Bonal, D., Steppe, K., and Ciais, P.: Seasonal patterns of CO₂ fluxes in Amazon forests: fusion of eddy covariance data and the ORCHIDEE model, *J. Geophys. Res.*, 116, G02018, doi:10.1029/2010JG001544, 2011.

Vermote, E. F., El Saleous, N. Z., and Justice, C. O.: Atmospheric correction of MODIS data in the visible to middle infrared: first results, *Remote Sens. Environ.*, 83, 97–111, doi:10.1016/S0034-4257(02)00089-5, 2002.

20 Vermote, E. F., Justice, C. O., and Breon, F.-M.: Towards a generalized approach for correction of the BRDF effect in MODIS directional reflectances, *IEEE T. Geosci. Remote*, 47, 898–908, doi:10.1109/TGRS.2008.2005977, 2009.

25 von Randow, C., Manzi, A. O., Kruijt, B., Oliveira, P. J. de, Zanchi, F. B., Silva, R. L., Hodnett, M. G., Gash, J. H. C., Elbers, J. A., Waterloo, M. J., Cardoso, F. L., and Kabat, P.: Comparative measurements and seasonal variations in energy and carbon exchange over forest and pasture in South West Amazonia, *Theor. Appl. Climatol.*, 78, 5–26, doi:10.1007/s00704-004-0041-z, 2004.

Wang, Y.-P., Leuning, R., Cleugh, H. A., and Coppin, P. A.: Parameter estimation in surface exchange models using nonlinear inversion: how many parameters can we estimate and which measurements are most useful?, *Glob. Change Biol.*, 7, 495–510, 2001.

30 Wang, Y. P., Baldocchi, D., Leuning, R., Falge, E., and Vesala, T.: Estimating parameters in a land-surface model by applying nonlinear inversion to eddy covariance flux measurements from eight FLUXNET sites, *Glob. Change Biol.*, 13, 652–670, doi:10.1111/j.1365-2486.2006.01225.x, 2007.

Generic model optimization across ecosystems**S. Kuppel et al.**[Title Page](#)[Abstract](#)[Introduction](#)[Conclusions](#)[References](#)[Tables](#)[Figures](#)[Back](#)[Close](#)[Full Screen / Esc](#)[Printer-friendly Version](#)[Interactive Discussion](#)

Wilkinson, M., Eaton, E. L., Broadmeadow, M. S. J., and Morison, J. I. L.: Inter-annual variation of carbon uptake by a plantation oak woodland in south-eastern England, *Biogeosciences*, 9, 5373–5389, doi:10.5194/bg-9-5373-2012, 2012.

Williams, M., Richardson, A. D., Reichstein, M., Stoy, P. C., Peylin, P., Verbeeck, H., Carvalhais, N., Jung, M., Hollinger, D. Y., Kattge, J., Leuning, R., Luo, Y., Tomelleri, E., Trudinger, C. M., and Wang, Y. -P.: Improving land surface models with FLUXNET data, *Biogeosciences*, 6, 1341–1359, doi:10.5194/bg-6-1341-2009, 2009.

Wilson, T. B. and Meyers, T. P.: Determining vegetation indices from solar and photosynthetically active radiation fluxes, *Agr. Forest Meteorol.*, 144, 160–179, doi:10.1016/j.agrformet.2007.04.001, 2007.

Xu, T., White, L., Hui, D., and Luo, Y.: Probabilistic inversion of a terrestrial ecosystem model: analysis of uncertainty in parameter estimation and model prediction, *Global Biogeochem. Cy.*, 20, GB2007, doi:10.1029/2005GB002468, 2006.

Zha, T., Barr, A. G., Black, T. A., McCaughey, J. H., Bhatti, J., Hawthorne, I., Krishnan, P., Kidston, J., Saigusa, N., Shashkov, A., and Nesic, Z.: Carbon sequestration in boreal jack pine stands following harvesting, *Glob. Change Biol.*, 15, 1475–1487, doi:10.1111/j.1365-2486.2008.01817.x, 2009.

5

10

15

Generic model optimization across ecosystems

S. Kuppel et al.

[Title Page](#)

[Abstract](#)

[Introduction](#)

[Conclusions](#)

[References](#)

[Tables](#)

[Figures](#)

[◀](#)

[▶](#)

[◀](#)

[▶](#)

[Back](#)

[Close](#)

[Full Screen / Esc](#)

[Printer-friendly Version](#)

[Interactive Discussion](#)



Table 1. Parameters of ORCHIDEE optimized in this study. The prior values are given for each PFT (see acronyms in Table 2), and multi-site posterior values are underlined. A hyphen means that the parameter is not optimized, *spinup* that the spinup value is taken, and **site** that the posterior value is site-specific.

Parameter	Description	Plant functional type						
		Trop EBF	Temp ENF	Temp EBF	Temp DBF	Bor ENF	Bor DBF	C ₃ grass
Photosynthesis								
V _{cmax}	Maximum carboxylation rate ($\mu\text{mol m}^{-2} \text{s}^{-1}$)	65 70.28	35 31.94	45 47.84	55 55.83	35 32.36	45 32.97	70 51.10
G _{s, slope}	Ball-Berry slope	9 8.756	9 8.841	9 10.99	9 6.000	9 7.961	9 7.714	9 9.970
C _{Tmax}	Offset controlling the maximum photosynthesis temperature (°C)	55 55.31	38 40.41	48 49.66	38 36.09	38 36.42	38 36.70	41.13 40.20
C _{Topt}	Offset controlling the optimal photosynthesis temperature (°C)	37 35.93	25 17.49	32 28.82	26 28.44	25 26.48	25 28.71	27.25 29.76
C _{Tmin}	Offset controlling the minimal photosynthesis temperature (°C)	2 1.356	-4 -7.536	-3 -6.062	-2 -0.219	-4 -6.167	-4 -2.563	-3.25 -3.403
Phenology								
SLA	Specific leaf area (foliar surface per dry matter content, $\text{m}^2 \text{g}^{-1}$)	0.0154 0.0169	0.0093 0.0200	0.02 0.0252	0.026 0.0400	0.0093 0.0090	0.0260 0.0233	0.0260 0.0345
LAI _{MAX}	Maximum LAI ($\text{m}^2 \text{m}^{-2}$)	7 7.000	5 5.000	5 5.000	5 3.949	4.5 4.500	4.5 4.960	4.5 2.349
K _{lai, happy}	Minimum fraction of LAI _{MAX} to stop carbohydrate use	0.5 0.500	0.5 0.500	0.5 0.500	0.5 0.321	0.5 0.500	0.5 0.547	0.5 0.408
K _{pheno, crit}	Multiplicative factor for growing season start threshold	— —	— —	— —	1 1.510	— —	1 0.758	1 0.729
C _{T,senes}	Offset controlling the temperature threshold for senescence (°C)	— —	— —	— —	12 14.36	— —	7 7.899	— —
L _{agecrit}	Critical age for leaves (days)	730 717.9	910 1084	730 709.2	180 165.1	910 790.5	180 163.3	120 113.9
LAI _{init}	Initial LAI ($\text{m}^2 \text{m}^{-2}$)	spinup site	spinup site	spinup site	—	spinup site	—	spinup site
Soil water availability								
f _{stressh}	Parameter reducing the hydric limitation of photosynthesis	6 6.507	6 7.146	6 7.135	6 5.039	6 4.881	6 5.505	6 5.131

Generic model optimization across ecosystems

S. Kuppel et al.

[Title Page](#)

[Abstract](#)

[Introduction](#)

[Conclusions](#)

[References](#)

[Tables](#)

[Figures](#)



[Back](#)

[Close](#)

[Full Screen / Esc](#)

[Printer-friendly Version](#)

[Interactive Discussion](#)



Table 1. Continued.

Parameter	Description	Plant functional type						
		Trop EBF	Temp ENF	Temp EBF	Temp DBF	Bor ENF	Bor DBF	C ₃ grass
Dpu _{cste}	Total depth of the soil water reservoir (m)	2 2.377	2 2.387	2 1.536	2 0.959	2 2.012	2 2.303	2 1.865
Hum _{cste}	Parameter describing the exponential root profile (m ⁻¹)	0.8 0.718	1 1.102	0.8 0.743	0.8 1.577	1 1.874	1 0.676	4 2.800
Autotrophic respiration								
MR _a	Slope of the temperature dependence	0.16 0.105	0.16 0.127	0.16 0.156	0.16 0.094	0.16 0.185	0.16 0.178	0.16 0.174
MR _b	Offset of the temperature dependence of maintenance respiration	1 0.929	1 0.772	1 0.928	1 0.622	1 0.710	1 1.212	1 1.140
GR _{frac}	Fraction of biomass available for growth respiration	0.28 0.269	0.28 0.250	0.28 0.265	0.28 0.206	0.28 0.303	0.28 0.301	0.28 0.317
Heterotrophic respiration								
K _{soilC}	Scaling factor for all initial soil carbon stocks after spinup	1 site						
Q ₁₀	Factor of the temperature control function	1.994 2.119	1.994 1.676	1.994 2.067	1.994 2.182	1.994 2.879	1.994 2.663	1.994 2.778
HR _{H,b}	Parameter of the soil/litter moisture control function	2.4 2.356	2.4 2.387	2.4 2.343	2.4 2.191	2.4 2.503	2.4 2.457	2.4 2.489
HR _{H,c}	Offset of the soil/litter moisture control function	-0.29 -0.332	-0.29 -0.272	-0.29 -0.329	-0.29 -0.544	-0.29 -0.192	-0.29 -0.252	-0.29 -0.304
Decomposition								
<i>h</i> _{crit, litter}	Total litter height (m)	0.08 0.0697	0.08 0.0434	0.08 0.0613	0.08 0.0200	0.08 0.0213	0.08 0.114	0.08 0.0358
Z _{decomp}	Factor of the exponential profile of soil temperature and moisture	0.2 0.371	0.2 0.649	0.2 0.175	0.2 0.142	0.2 0.662	0.2 0.474	0.2 0.448
Energy balance								
K _{albedo, veg}	Multiplicative factor of surface albedo	1 1.031	1 1.042	1 0.930	1 1.110	1 1.076	1 1.048	1 0.989
Z _{0_overheight}	Reference roughness length (m)	0.0625 0.0648	0.0625 0.0877	0.0625 0.0359	0.0625 0.0200	0.0625 0.0200	0.0625 0.0513	0.0625 0.0200

Generic model optimization across ecosystems

S. Kuppel et al.

[Title Page](#)

[Abstract](#)

[Introduction](#)

[Conclusions](#)

[References](#)

[Tables](#)

[Figures](#)



[Back](#)

[Close](#)

[Full Screen / Esc](#)

[Printer-friendly Version](#)

[Interactive Discussion](#)



Table 2. Sites used in this study, with their name code made from the country (first two letters) and site name (last three letters).

PFT ^a	Site	Latitude	Longitude	Period	Reference
TropEBF	BR-Ban	-9.824	-50.159	2004–2005	da Rocha et al. (2009)
	BR-Cax	-1.720	-51.459	2000–2002	Carswell et al. (2002)
	BR-Ji2	-10.083	-61.931	2000–2002	Randow et al. (2004)
	BR-Sa3	-3.018	-54.971	2001–2002	Goulden et al. (2004)
	ID-Pag	2.345	114.036	2002–2003	Hirano et al. (2007)
TempENF	CA-Ca3	49.535	-124.900	2002	Jassal et al. (2008)
	CA-TP4	42.710	-80.357	2004	Arain and Restrepo-Coupe (2005)
	DE-Bay	50.142	11.867	1998–1999	Staudt and Foken (2007)
	DE-Tha	50.964	13.567	1997–2003	Grünwald and Bernhofer (2007)
	DE-Wet	50.453	11.458	2002–2006	Rebmann et al. (2010)
	FR-Lbr	44.717	-0.769	2003–2006	Berbigier et al. (2001)
	IT-Lav	45.955	11.281	2004	Marcolla et al. (2003)
	IT-Ren	46.588	11.435	2002	Montagnani et al. (2009)
	IT-SRo	43.728	10.284	2002–2004	Chiesi et al. (2005)
	NL-Loo	52.168	5.744	2001–2002	Dolman et al. (2002)
	SE-Nor	60.086	17.480	1996–1997	Lagergren et al. (2008)
	SE-Sk1	60.125	17.918	2005	Gioli et al. (2004)
	SE-Sk2	60.130	17.840	2005	
	UK-Gri	56.607	-3.798	2000–2001	Clement et al. (2012)
	US-Ho1	45.204	-68.740	2003–2004	Hollinger et al. (2004)
	US-Ho2	45.209	-68.747	1999–2004	Davidson et al. (2006)
	US-Me2	44.452	-121.557	2004–2005	Anthoni et al. (2002)
	US-Me4	44.499	-121.622	2000	Anthoni et al. (2002)
	US-NC2	35.803	-76.668	2005–2006	Noormets et al. (2010)
	US-Wrc	45.820	-121.952	1999–2002	Falk et al. (2008)
TempEBF	AU-Tum	-35.656	148.152	2001–2003	Leuning et al. (2005)
	AU-Wac	-37.429	145.187	2006	Kilinc et al. (2013)
TempDBF	DE-Hai	51.079	10.452	2000–2006	Mund et al. (2010)
	FR-Fon	48.476	2.780	2006	Michelot et al. (2011)
	FR-Hes	48.674	7.065	2001–2003	Granier et al. (2008)
	JP-Tak	36.146	137.423	1999–2004	Ito et al. (2006)
	UK-Ham	51.121	-0.861	2004–2005	Wilkinson et al. (2012)
	US-Bar	44.065	-71.288	2004–2005	Jenkins et al. (2007)
	US-Ha1	42.538	-72.172	2003–2006	Urbanski et al. (2007)
	US-LPH	42.542	-72.185	2003–2004	Hadley et al. (2008)
	US-MOz	38.744	-92.200	2005–2006	Gu et al. (2012)
	US-UMB	45.560	-84.714	2000–2003	Nave et al. (2011)
	US-WCr	45.806	-90.080	1999–2004	Cook et al. (2004)

Table 2. Continued.

PFT ^a	Site	Latitude	Longitude	Period	Reference
BorENF	CA-Man	55.880	-98.481	1998–2003	Dunn et al. (2007)
	CA-NS1	55.879	-98.484	2003–2004	Goulden et al. (2006)
	CA-NS2	55.906	-98.525	2002–2004	Goulden et al. (2006)
	CA-NS3	55.912	-98.382	2002–2004	Goulden et al. (2006)
	CA-Obs	53.987	-105.118	2000–2005	Krishnan et al. (2008)
	CA-Ojp	53.916	-104.692	2000–2005	Howard et al. (2004)
	CA-Qfo	49.693	-74.342	2004–2006	Bergeron et al. (2007)
	CA-SJ3	53.876	-104.645	2005	Zha et al. (2009)
	FI-Hyy	61.847	24.295	1997–2006	Suni et al. (2003)
	FI-Sod	67.362	26.638	2001–2006	Sánchez et al. (2009)
	SE-Fla	64.113	19.457	2001–2002	Lindroth et al. (2008)
	US-Bn1	63.920	-145.378	2003	Liu et al. (2005)
BorDBF	US-NR1	40.033	-105.546	2002–2003	Sacks et al. (2006)
	CA-Oas	53.629	-106.198	2001–2004	Black et al. (2000)
	SE-Abi	68.362	18.795	2005	Christensen et al. (2007)
C3grass	US-Bn2	63.920	-145.378	2003	Liu et al. (2005)
	CA-Let	49.709	-112.940	1999–2005	Flanagan and Atkinson (2011)
	CA-NS6	55.917	-98.964	2002–2004	Goulden et al. (2006)
	CA-NS7	56.636	-99.948	2003–2004	Goulden et al. (2006)
	CN-HaM	37.370	101.180	2002–2003	Kato et al. (2006)
	DE-Meh	51.275	10.656	2004–2005	Don et al. (2009)
	ES-LMa	39.942	-5.773	2004–2005	
	ES-VDA	42.152	1.449	2004	Gilmanov et al. (2007)
	HU-Bug	46.691	19.601	2003–2006	Nagy et al. (2007)
	HU-Mat	47.847	19.726	2004–2006	Pintér et al. (2008)
	IE-Dri	51.987	-8.752	2003–2004	Peichl et al. (2011)
	IT-Amp	41.904	13.605	2005	Gilmanov et al. (2007)
	IT-Mal	46.117	11.703	2003–2004	Gilmanov et al. (2007)
	IT-MBo	46.016	11.047	2004–2006	Gianelle et al. (2009)
	NL-Ca1	51.971	4.927	2003–2004	Jacobs et al. (2007)
	NL-Hor	52.029	5.068	2004–2006	Hendriks et al. (2007)
	SE-Deg	64.183	19.550	2001–2005	Sagerfors et al. (2008)
	US-ARM	36.605	-97.488	2003–2005	Fischer et al. (2007)
	US-Aud	31.591	-110.510	2005	Wilson and Meyers (2007)
	US-Bkg	44.345	-96.836	2005–2006	Gilmanov et al. (2005)
	US-Bn3	63.923	-145.744	2003	Liu et al. (2005)
	US-Goo	34.250	-89.970	2004	Wilson and Meyers (2007)
	US-IB2	41.841	-88.241	2006	Allison et al. (2005)
	US-Ivo	68.487	-155.750	2004–2005	Oechel et al. (2000)
	US-Var	38.413	-120.951	2002	Ma et al. (2007)

^a TropEBF: tropical evergreen broadleaf forest; TempENF: temperate evergreen needleleaf forest; TempEBF: temperate evergreen broadleaf forest; TempDBF: temperate deciduous broadleaf forest; BorENF: boreal evergreen needleleaf forest; BorDBF: boreal deciduous broadleaf forest; C3grass: C₃ grassland.

Generic model optimization across ecosystems

S. Kuppel et al.

Title Page

Abstract

Introduction

Conclusions

References

Tables

Figures



Back

Close

Full Screen / Esc

Printer-friendly Version

Interactive Discussion



Generic model optimization across ecosystems

S. Kuppel et al.

Table 3. Median Pearson correlation factors between measured NDVI and modeled FAPAR at the global scale, during the period 2000–2010.

PFT	Median correlation factor	
	Prior	Multi-site
TropEBF	0.09	0.10
TempENF	0.52	0.55
TempEBF	0.56	0.62
TempDBF	0.90	0.93
BorENF	0.48	0.60
C3grass	0.49	0.53
All PFTs	0.56	0.59



Generic model optimization across ecosystems

S. Kuppel et al.

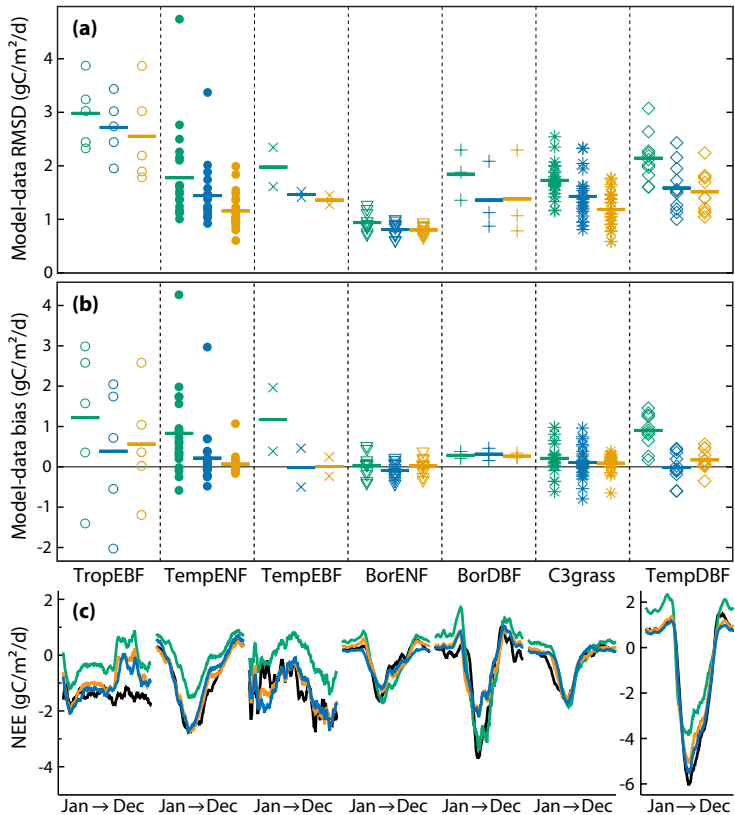


Fig. 1. Model-data **(a)** RMSD and **(b)** bias, and **(c)** PFT-averaged mean seasonal cycle of NEE. In **(a)** and **(b)**, the horizontal lines give for each PFT the average of the individual site values (symbols), in three cases: prior model (green), multi-site optimization (blue) and single-site optimization (orange). In **(c)**, the seasonal cycles of observations (black) and simulations are smoothed with a 15 day-moving-average window.

Generic model optimization across ecosystems

S. Kuppel et al.

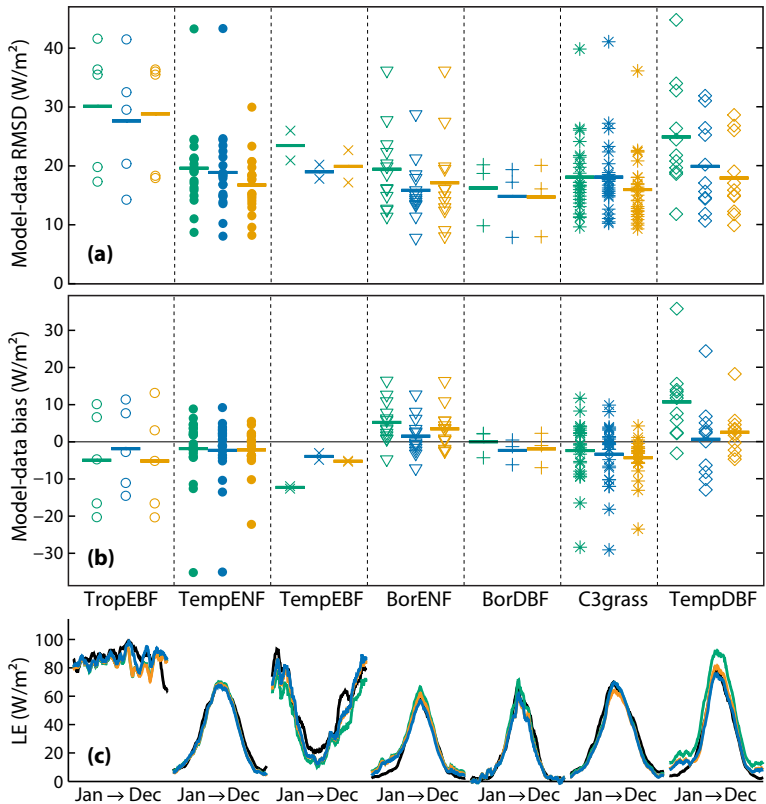


Fig. 2. Model-data **(a)** RMSD and **(b)** bias, and **(c)** PFT-averaged mean seasonal cycle of LE. In **(a)** and **(b)**, the horizontal lines give for each PFT the average of the individual site values (symbols), in three cases: prior model (green), multi-site optimization (blue) and single-site optimization (orange). In **(c)**, the seasonal cycles of observations (black) and simulations are smoothed with a 15 day-moving-average window.

Generic model optimization across ecosystems

S. Kuppel et al.

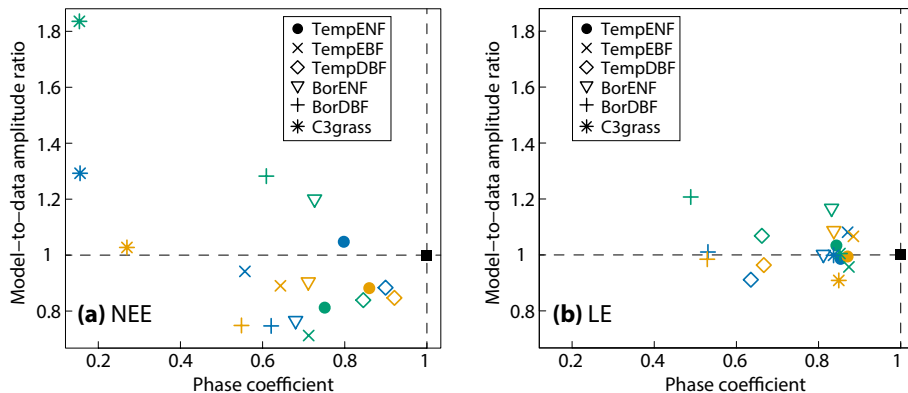


Fig. 3. PFT-averaged model phase coefficient vs. model-to-data amplitude ratio, for (a) NEE and (b) LE fluxes. Simulations using prior parameters (green) are compared to single-site (orange) and multi-site (blue) optimizations, with the measured reference indicated by the black square.

Generic model optimization across ecosystems

S. Kuppel et al.

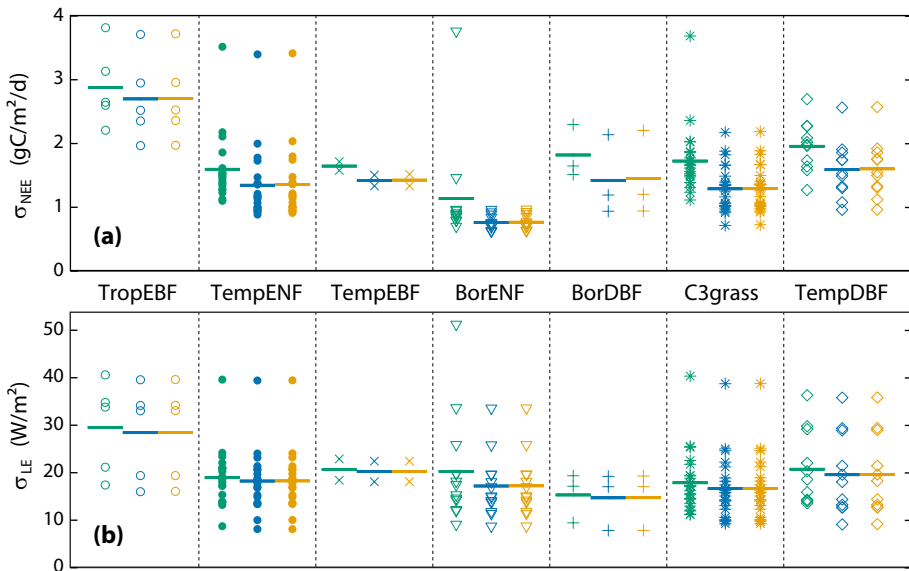


Fig. 4. Uncertainty of simulated daily (a) NEE and (b) LE fluxes. For each PFT, the horizontal lines give the average of the individual site values (symbols), in three cases: prior model (green), multi-site optimization (blue) and single-site optimization (orange).

Generic model optimization across ecosystems

S. Kuppel et al.

Title Page

Abstract

Introduction

Conclusion

Conclusions | References

Conclusions | References

Conclusions | References

Tables

Figures

1

1

Back

Close

Full Screen / Esc

Printer friendly Version

Interactive Discussion

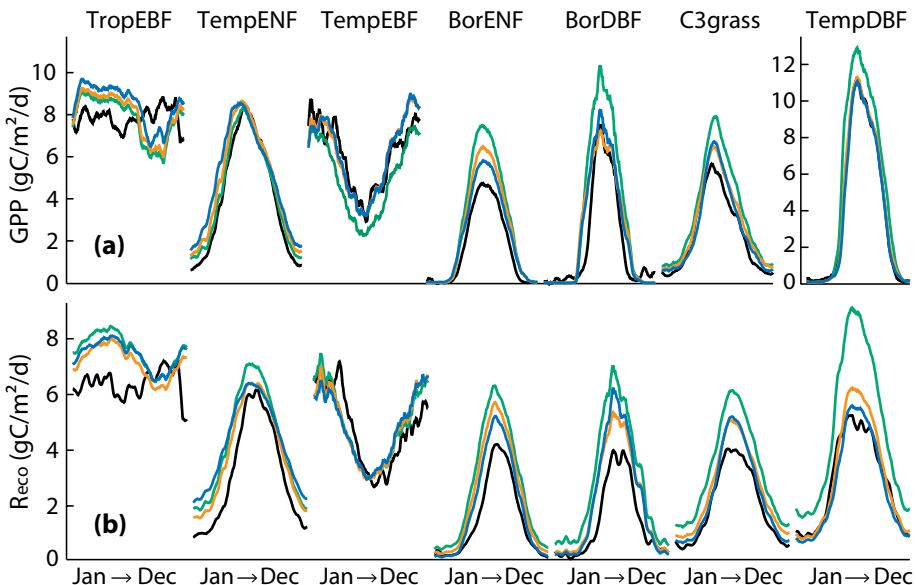


Fig. 5. PFT-averaged mean seasonal cycles of **(a)** the photosynthetic carbon flux and **(b)** the respiration flux, smoothed with a 15 day-moving-average window. Observations (black) are compared to the simulations using prior (green), single-site (orange) and multi-site (blue) parameterizations.

Generic model optimization across ecosystems

S. Kuppel et al.

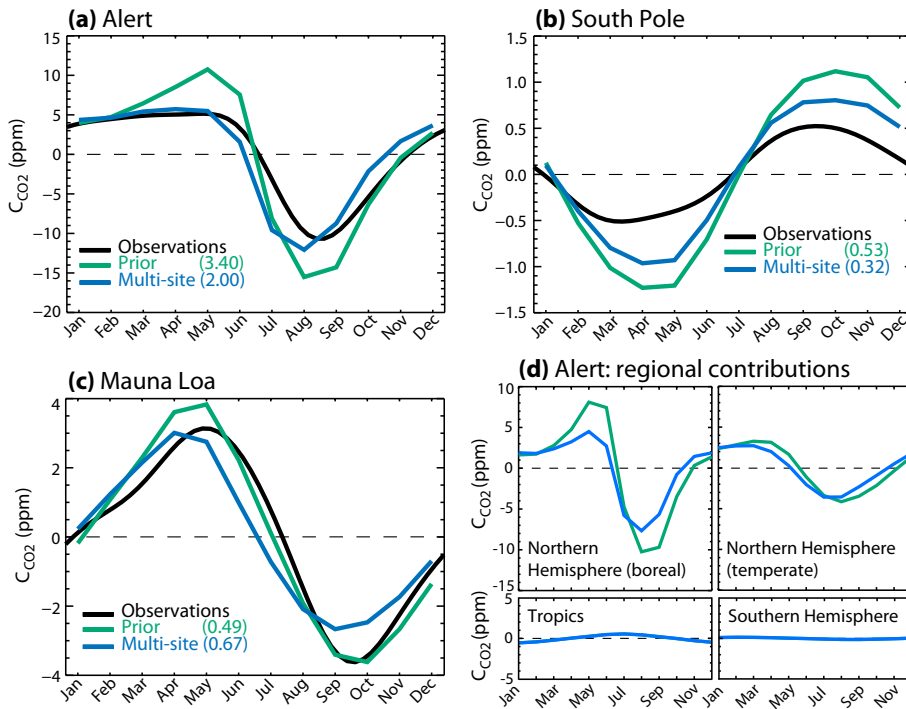


Fig. 6. Detrended mean seasonal cycle of the atmospheric CO₂ concentrations at **(a)** Alert, **(b)** South Pole and **(c)** Mauna Loa locations: the measured concentrations (black) are compared to simulations where the biospheric contribution is calculated using the ORCHIDEE model with default (green) and multi-site (blue) parameterization, with the model–data RMSD given between brackets. **(d)** Regional contributions to the mean seasonal cycle simulated at Alert.